A review of the state of research on wave-current interaction in nearshore areas

Xuan Zhang[1,2,3], Richard Simons[2], Jinhai Zheng[1,3], Chi Zhang[1]
1. College of Harbor, Coastal and Offshore Engineering, Hohai University, Nanjing, China
2. Department of Civil, Environmental and Geomatic Engineering, University College London, Gower Street, London, WC1E 6BT, UK
3. Key Laboratory of Ministry of Education for Coastal Disaster and Protection, Hohai University, Nanjing, China

Abstract: The interaction between currents and ocean waves is a physical process commonly occurring in coastal environments and is of importance for designers of offshore structures, engineers concerned with sediment transport and dispersion of pollutants. To provide scientists and engineers with a summary of existing knowledge on the topic, this paper presents a review of the state of the art of studies into the interaction between water waves and turbulent currents. The progress of our understanding of this issue is reviewed, together with an overview of experimental and numerical investigations. In particular, a synopsis of advantages and limitations of previous studies is included, together with suggestions for future studies in the field.
Keywords: Water waves, turbulent current, Wave-current interaction, boundary layers, experiments, numerical modelling.

1. Introduction

In coastal areas, surface gravity waves and ocean currents are often experienced at the same time. The waves are usually generated by wind, while the currents can be generated by, for example, waves, density variations, and tides. The interaction between waves and currents are of vital significance to coastal engineers concerned with hydrodynamics in near-shore regions. Hydrodynamic loading of coastal structures, scouring around offshore structures, flow fields near pipelines, and dispersal of pollutants are all typical examples which require an enhanced understanding of wave-current interaction.

In nature, currents are normally turbulent; a turbulent boundary layer is characterized by its ability to mix and transport fluid across several layers. Physically, the interaction of ocean waves with a turbulent current is complicated by the various temporal and spatial scales created by the two processes. For instance, the thickness of a current-induced turbulent boundary layer is normally in the order of magnitude of the water depth, while wave boundary layers are typically limited to the region very close to the bed. An illustration of velocity profiles induced by these two components is shown in Figure 1. This shows that waves dominate the near-bed flow, even if the current-induced velocity is larger than the wave-induced velocity magnitude near the free surface.

The topic of wave-current interaction (WCI), a term generally referring to the kinematics (velocity field) and dynamics (bed shear stress) induced by the interaction between oscillatory waves and a turbulent current, has received considerable attention in the past few decades because of its engineering applications as stated above. Quantitative experiments have been carried out to study the interaction between waves and a turbulent current, including:

i. wave kinematics such as wave length, wave height, wave energy spectrum etc. changed by current;
ii. radiation stresses generated by waves, which give rise to currents;
iii. mean velocity profiles altered by wave motions;
iv. turbulent characteristics altered by wave motion;

v. bed shear stresses under combined wave and current conditions, which are closely related with sediment transport.

The first issue has been investigated since 1960. Previous studies have shown that a following (opposing) current results in decreased (increased) wave heights and increased (decreased) wave lengths. This phenomenon is related to the Doppler shift theory, and theoretical investigations have been made by many researchers using the dispersion relation (Jonsson et al., 1970; Peregrine, 1976; Brevik and Aas, 1980; Thomas, 1981, 1990; Tolman, 1990; Hedges and Lee, 1992; Yang and Liu, 2020). Experimental results have shown that the changes in wavelengths and wave heights can be well predicted by the theory. Brevik (1980) measured the wave heights and wavelengths in a laboratory flume over a smooth bed. Their experimental results showed good agreements with the theoretical values described by Brevik and Aas (1980), applicable to waves interacting with non-uniform steady currents. Thomas (1981; 1990) reported laboratory experiments for linear and nonlinear waves interacting with currents of arbitrary vorticity, further suggesting the validity of their theory. Large-scale laboratory experiments were conducted by Rusu and Soares (2011) using a 3D large wave basin. Analysis of the wave frequency spectra indicated that the following (opposing) current led to a decreased (increased) significant wave height. More recently, Hashemi et al. (2016) determined changes in wave heights and wave lengths induced by the ambient current, based on the linear wave theory. Field data from the UK shelf and in the Bristol Channel were collected and used for validation. For a comprehensive review dealing with this perspective, see Peregrine (1976), Grant and Madsen (1986), Jonsson (1990), Sleath (1990b), and Wolf and Prandle (1999).

Radiation stresses have been widely adopted to model WCI since originally put forward by Longuet-Higgins (1962, 1964). Two-dimensional radiation stress models (Phillips, 1977; Smith, 2006) were later generalised to three-dimensional models by many researchers. Mellor (2003) presented surface wave equations applicable to three-dimensional ocean models. This model was revised by Mellor (2008) to include some missing terms, and the momentum equation was not sensitive to finite horizontal derivatives of the bottom depth. However, Bennis and Ardhuin (2011) concluded that the model of Mellor (2008) was inconsistent with the depth-integrated momentum balance. Unrealistic surface elevations and currents were detected in the absence of dissipation. The currents may reach significant values for very moderate waves, exceeding the expected results by one order of magnitude. The spurious velocities produced by the model of Mellor (2008) were ascribed to the use of different averaging for the pressure gradient term and for the advection terms of the same equation. The models of Ardhuin et al. (2008b) and McWilliams et al. (2004), however, do not have such problems and are therefore better than Mellor (2008). Mellor (2011) further derived vertically dependent radiation stresses to overcome the shortcoming of Mellor (2003) when dealing with pressure terms. Based on the vertically Lagrangian coordinate system proposed by Mellor (2003, 2008), Aiki and Greatbatch (2012) further developed depth-dependent equations for waves and currents in a vertically Lagrangian and horizontally Eulerian (VL) coordinate system. All these works led to a debate concerning the applicability of the Mellor approach to a sloping bottom. Aiki and Greatbatch (2013) addressed this issue and solved the problem by deriving the depth-dependent radiation stress in vertically Lagrangian and horizontally Eulerian (VL) coordinates. Mellor (2015) provided a review of the vertically integrated wave circulation equations and derived simpler vertically dependent WCI equations, based on the theory of Mellor (2003). Ardhuin et al. (2008) further suggested a numerical correction method since analytical expressions for the pressure and coordinate transformation function were not given by Mellor (2003). More recently, Zheng et al. (2020) performed laboratory experiments in a wave basin to better understand the wave-induced setup and wave-driven current. Wave setup is observed to be dependent on the radiation

stress, which is strongly influenced by the bathymetry and water depth. Results suggest that larger onshore current can lead to an enhanced reduction of wave set-up on the reef flat due to WCI.

In this paper, we are focused on aspects iii-v. Previous studies have identified the non-linear characteristics of WCI. Many analytical models of WCI are based on the eddy viscosity assumption to relate the mean velocity profile and Reynolds shear stress, adopting a variety of eddy viscosity distributions through the boundary layer. The accurate prediction of bed shear stress is essential for modelling the coastal environment because bed shear stress is the driving mechanism for sediment transport and contributes to energy dissipation. In oscillatory boundary layers, different applications require knowledge of the maximum and the time-averaged mean values of bed shear stress. The maximum bed friction determines the initiation and entrainment of sediment, whereas the mean value drives the diffusion of suspended particle. The non-linear interaction between currents and waves leads, in most cases, to an enhancement of bed shear stress.

There are many engineering applications of WCI, which motivates the present work. One of the most significant impacts of wave-current interaction on the continental shelf is its effect on sediment transport rates (e.g. Zhang et al., 2014; Zheng et al., 2014) and, thereby, the evolution of coastal morphology. This impact occurs through two fundamental mechanisms: the change in eddy viscosity coefficient and the enhancement of bed shear stress. An accurate distribution of eddy viscosity is important for coastal modelling, as can be seen from the definition of eddy viscosity. The eddy viscosity assumption is also widely adopted for sediment transport modelling. Calculation of suspended sediment concentration (SSC) requires an accurate description of sediment diffusivity, which is related to the eddy viscosity typically representing the diffusivity of momentum (diffusion of a fluid ‘particle’). The entrainment of sediment is controlled by the maximum bed shear stress, and the diffusion of suspended particles is driven by the mean stress. Therefore, accurate predictions of instantaneous bed shear stress in WCI are important for the prediction and modelling of sediment transport. Proper estimations of the bed shear stress enhancement depend on whether the field conditions are wave-dominated or current-dominated, and coastal engineers require accurate values of waves and currents when estimating sediment transport rates.

A sound understanding of WCI is also important for the prediction of seabed scour around marine structures such as piers and offshore wind turbines. Scour occurs at structures situated in flowing water where there is potential for seabed sediments to be eroded. Enhanced bed shear stress caused by the acceleration of flow around the structure is the necessary driving force to entrain sediment particles from the seabed local to the foundation. As more sediment is transported downstream over time, a scour hole forms at the base of the structure. This can have critical consequences for the stability of the whole structure due to exposure or undermining of the foundation. In extreme cases this can result in structural failure, substantial financial losses and potential loss of life. The nonlinear interaction between waves and currents produces changes in flow velocities, bed shear stresses and vortex shedding that increase or mitigate the scour process.

Coastal engineers should be aware of the phenomenon that wave heights decrease (increase) for following (opposing) currents as induced by WCI and choose a proper WCI model to estimate their design conditions, i.e. design wave height. For instance, investigations have shown the strong WCI at the Columbia River Mouth, USA, using remote sensing data (Gonzalez and Rosenfeld, 1984) and numerical simulations (Kassem and Ozkan-Haller, 2012), who further observed the significance of WCI in accurate predictions of wave breaking. Akan et al. (2017) also looked at the Columbia River mouth, adopting the COAWST modelling system to investigate the WCI dynamics. Wave heights were observed to be intensified significantly at the river mouth when tidal currents were present.

Potential enhanced dispersion of pollutant plumes can also be induced by WCI, since wave breaking has been suggested to be a mechanism for enhanced plume mixing. The plume may be thicker, taking into account the effects of wave breaking and turbulence under the influence of WCI. Transport of sewage, dredging spoil and pollutants at power station outfalls etc. under the effects of WCI can ultimately impact water quality, marine life, and public health along the coastlines. Therefore, it is important to provide an accurate knowledge of WCI and predict the structure of such pollutant plumes.

The understanding of WCI is essential in the design of offshore structures. Hydrodynamic loading is frequently due to combined waves and currents, and nonlinear interactions between them can have a significant effect on design conditions. Any improvement in the description of the water particle motions will lead to a more accurate estimate of the fluid loading on marine and offshore structures.

Knowledge of WCI is also useful in the initial location and development stages of marine renewable energy projects. For instance, turbine designers need to assess energy yield and fatigue loading taking account of wave-induced changes to the characteristics of the currents, while currents can change the height and direction of the waves. The technical suggestions given by the Turbulence in Marine Environments (TiME) project (Clark et al., 2015) show that turbine loading and power performance are highly sensitive to both turbulence fluctuations and mean velocity profiles. The turbulence characteristics of a combined wave-current flow must thus be given precisely so as to adequately estimate energy yield and hydrodynamic loading induced by the turbulent flow.

The present review paper summarises existing knowledge of WCI. Section 2 reviews basic theories describing the flow field of WCI. In particular, theories proposed so far to explain the WCI mechanism are considered. Experimental studies are included in section 3, in terms of laboratory experiments and field tests. Conclusions regarding the present knowledge of WCI are given in section 4, with some suggestions for future developments of the subject given at the end.

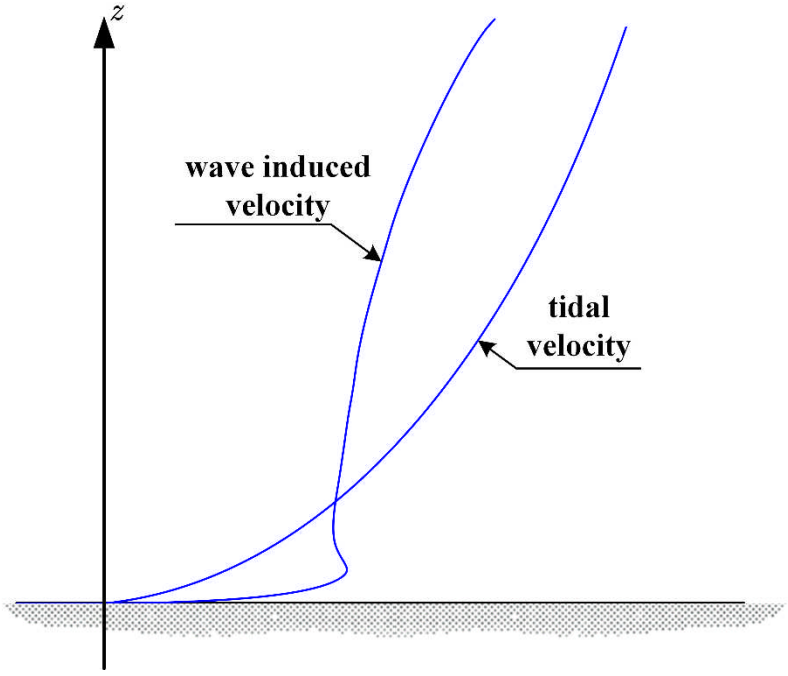

Figure 1. Velocity distributions induced by waves and a tidal current, from Nielsen (1992).

2. Theoretical background

The basic equations governing the motions of a combined wave-current flow are the Navier-

Stokes equations (N-S equations). These are composed of the continuity, momentum, and energy equations. The continuity and momentum equations for incompressible fluid are given as follows:

$$\frac{\partial u}{\partial x} + \frac{\partial v}{\partial y} + \frac{\partial w}{\partial z} = 0 \qquad \text{Equation 1}$$

$$\frac{\partial(\rho u)}{\partial t} + \rho u\frac{\partial u}{\partial x} + \rho v\frac{\partial u}{\partial y} + \rho w\frac{\partial u}{\partial z} = -\frac{\partial p}{\partial x} + \nu\left(\frac{\partial^2 u}{\partial x^2} + \frac{\partial^2 u}{\partial y^2} + \frac{\partial^2 u}{\partial z^2}\right) + f_x \qquad \text{Equation 2}$$

$$\frac{\partial(\rho v)}{\partial t} + \rho u\frac{\partial v}{\partial x} + \rho v\frac{\partial v}{\partial y} + \rho w\frac{\partial v}{\partial z} = -\frac{\partial p}{\partial x} + \nu\left(\frac{\partial^2 v}{\partial x^2} + \frac{\partial^2 v}{\partial y^2} + \frac{\partial^2 v}{\partial z^2}\right) + f_y \qquad \text{Equation 3}$$

$$\frac{\partial(\rho w)}{\partial t} + \rho u\frac{\partial w}{\partial x} + \rho v\frac{\partial w}{\partial y} + \rho w\frac{\partial w}{\partial z} = -\frac{\partial p}{\partial x} + \nu\left(\frac{\partial^2 w}{\partial x^2} + \frac{\partial^2 w}{\partial y^2} + \frac{\partial^2 w}{\partial z^2}\right) + f_z \qquad \text{Equation 4}$$

where p represents static pressure; x, y, z are the Cartesian coordinates: x for the streamwise direction, z for the vertical one; u, v, w are the corresponding velocity components; ρ represents the density; t is time; ν represents kinematic viscosity and f_x, f_y, f_z are the body forces (including any source terms).

The corresponding equations for a combined wave-current motion can then be derived by substituting the expressions for velocity and pressure components into the basic N-S equations. Note that here in a combined flow, the velocity component in each direction includes a periodic component as well as the steady and the random ones. This is also valid for the pressure component. In general, these are expressed by the following equations:

$$u = \bar{u} + \tilde{u} + u' \qquad \text{Equation 5}$$

$$v = \bar{v} + \tilde{v} + v' \qquad \text{Equation 6}$$

$$w = \bar{w} + \tilde{w} + w' \qquad \text{Equation 7}$$

$$p = \bar{p} + \tilde{p} + p' \qquad \text{Equation 8}$$

In this paper, for a quantity M, $\bar{\mathrm{M}}$ is the time-average of M over the samples, $\widetilde{\mathrm{M}}$ is the periodic component, $\langle \mathrm{M} \rangle$ is the ensemble-average of M, and M' is the turbulent component:

$$\langle M \rangle = \frac{1}{J}\sum_{j=0}^{J-1} M(t + j \cdot T), \qquad 0 \le t < T \qquad \text{Equation 9}$$

$$\widetilde{M}(t) = \langle M \rangle - \bar{M}, \qquad 0 < t < T \qquad \text{Equation 10}$$

where T is wave period, J is the number of wave cycles for ensemble-averaging.

In order to solve the equations, different turbulence closure models have been adopted by many researchers in the field of WCI. These can be categorised into two main types: analytical approaches (with some simplifications of the N-S equations based on particular assumptions) and numerical methods. This will be further reviewed in the following sub-sections.

2.1 Analytical models

The earliest studies on WCI applied analytical approaches to investigate kinematics and dynamics of the bottom boundary layer under combined waves and currents. Such algebraic models are often referred to as 'zero-equation' models. The governing equation to determine the bed shear stress and the velocity components is the wave-current boundary layer equation, which considers only the horizontal component of flow in the x-z plane and assumes that the flow inside the boundary layer is essentially horizontal. See equation 11.

$$\frac{\partial u}{\partial t} = -\frac{1}{\rho}\frac{\partial p}{\partial x} + \frac{\partial}{\partial z}\left(\frac{\tau_{Rey}}{\rho}\right) \qquad \text{Equation 11}$$

where τ_{Rey} is the Reynolds shear stress.

This governing equation has been solved, based on the eddy viscosity concept as a positive scalar coefficient. This was put forward by Boussinesq (1877) by analogy to molecular viscosity to relate the Reynolds stress tensor and the mean strain rate tensor. In the case of a two-dimensional turbulent flow, the eddy viscosity can be defined as the coefficient of

proportionality linking Reynolds shear stress with the velocity gradient normal to the boundary. See equation 12.

$$\varepsilon_t = \frac{\tau_{Rey}/\rho}{\frac{\partial u}{\partial z}} \qquad \text{Equation 12}$$

where $\frac{\partial \mathrm{u}}{\partial z}$ is the velocity gradient normal to the boundary.

Zero-equation WCI models can be classified into five groups: time-invariant eddy viscosity models (Lundgren, 1972; Grant and Madsen, 1979; Myrhaug, 1982; Christoffersen and Jonsson, 1985; Myrhaug and Slaattelid, 1989; 1990; You et al., 1991; 1992; You, 1994a, 1994b; Yuan and Madsen, 2015; Tambroni et al., 2015), time-dependent eddy viscosity models (Malarkey and Davies, 1998), mixing length models (Umeyama, 2005; 2009), momentum-based models (Fredsøe, 1984), and parameterised models (Soulsby et al., 1993).

Different eddy viscosity assumptions have been put forward (see Figures 2 to 4 for graphs showing various eddy viscosity profiles). These figures show the distributions of eddy viscosities across prescribed layers. The first model of eddy viscosity in a combined wave-current flow was proposed by Lundgren (1972), who made the assumption that the current and the wave could be described by independent eddy viscosities. This model is only applicable to a wave-dominated condition because the characteristics of the wave boundary layer were determined from the wave-alone case, without considering the current effects. Based on the same concept, Grant and Madsen (1979) proposed a two-layer time-invariant turbulent eddy viscosity model (referred to as GM79 hereafter) to describe the combined motion and the associated bed shear stress near a rough boundary. The eddy viscosities are linearly varied with the distance from the bed, with different slopes in the two layers. This model was adapted by Myrhaug and Slaattelid (1990) to obtain the bottom friction coefficients for smooth, rough, and transitional turbulent flows. Malarkey and Davies (1998) modified the GM79 model by including the time variations in the eddy viscosity. More recently, Humbyrd (2012) further developed the GM79 model to overcome the discontinuity in the two layers. Yuan and Madsen (2015) found that the GM79 model cannot predict the current profile for nonlinear-wave-current flows. This is because the turbulence-asymmetry streaming, induced by the combined influence of the superimposed current and the wave nonlinearities, can greatly contaminate the basic current which follows the two-log-profile structure suggested by the GM79 model. Yuan and Madsen (2015) further developed the GM79 model by adopting a time-varying turbulent eddy viscosity. The model can predict the turbulence asymmetry streaming accurately. Thus, the model is applicable for currents interacting with linear or nonlinear waves. However, it should be noted that the model of Yuan and Madsen (2015) does not include the Longuet-Higgins-type streaming due to wave propagation. Therefore, there is scope to extend this study to applications in large scale circulation models.

Christoffersen and Jonsson (1985) proposed two different models applicable to the whole range of sea bed roughnesses, using different time-independent eddy viscosity distributions. The eddy viscosity for both models was the same in the outer region, both parabolic outside the wave boundary layer. In the vicinity of the sea bed, the eddy viscosity was assumed to be constant for a bed with large roughness and to linearly increase with the distance from the bed for cases of smaller roughness. Myrhaug and Slaattelid (1989) proposed a three-layer eddy viscosity model, where the eddy viscosity was parabolic in the inner layer and increased linearly with height in the outer layers, depending on the maximum shear velocity for the combined flow and the current shear velocity respectively for the two upper parts. This model is an extension of Myrhaug (1982), where a two-layer time invariant eddy viscosity model for a wave bottom boundary layer near a rough bed was put forward.

You et al. (1991) presented a theoretical model of the mean velocity profile in a combined wave-current flow, based on the independent current eddy viscosity and wave eddy viscosity. Here, near the bed, the current eddy viscosity was assumed to vary linearly with the distance from the bed; further out a constant value was used, and then linearly distributed in the outer layer. The wave eddy viscosity was assumed to be linearly distributed in the inner layer, and then constant to the edge of the wave bottom boundary layer. This work was further developed by You (1994a), combining the current eddy viscosity of You et al. (1991) and the wave eddy viscosity assumption of You et al. (1992). A further simplified three-layer eddy viscosity model was presented by You (1994b), where the eddy viscosity was linear within the wave bottom boundary layer, then constant in the overlap region, and linear again in the outer region. A parabolic or constant eddy viscosity was assumed by Nielsen and You (1996) to deduce the mean velocity profile. Detailed information describing many of the eddy viscosity models has been included in Nielsen (1992), and Fredsøe and Deigaard (1992).

The mixing length theory of Prandtl (1925), which was developed for a unidirectional turbulent current, was applied by Bakker and von Doorn (1978) to investigate the bottom boundary layer. Temporal variations inside the wave boundary layer were considered in their model. Similarly, Umeyama (2005) adopted the mixing length theory for WCI, based on a modified mixing length hypothesis developed by Umeyama and Gerritsen (1992). However, the temporal variations inside the wave boundary layer were not included.

Fredsøe (1984) used the momentum equation to study the bottom boundary layer. It was assumed that the time scales for the change in the outer velocity are much larger than those for the decay of eddies formed in the wave boundary layer. The theory was not valid at very high wave frequencies, where the history effects of turbulence formed in the previous half-cycle are no longer negligible.

A parameterised approach based on the outputs from most of these models was given by Soulsby et al. (1993) and Holmedal et al. (2000). Soulsby et al. (1993) reviewed the analytical models of Grant and Madsen (1979), Fredsøe (1984), Myrhaug and Slaattelid (1990), and Huynh-Thanh and Temperville (1991), and provided a mathematical representation of bed shear stress by curve fitting. This approach was adopted by Holmedal et al. (2000) and further generalised to the conditions of random waves propagating with a turbulent current. Bed shear stresses under irregular waves and currents were obtained, over a rough seabed. Results showed significant enhancement of the maximum bottom shear stress caused by the current, and were quantitatively in good agreement with laboratory and field measurements.

More recently, Tambroni et al. (2015) adopted a time-independent eddy viscosity model and a perturbation method to derive mean velocity distributions of combined flows. This was generalised to the condition where waves propagated with the current at an arbitrary angle.

The aforementioned analytical models provide a description of the interaction between waves and a turbulent current. Summaries of the keyword index of all these models are given in Appendices A to D. An enhanced bed shear stress (see Figure 5), together with altered velocity distributions are important phenomena in the case of combined waves and currents. Because turbulent shear stresses are not linearly proportional to velocities as in laminar flows, the turbulence generated by the waves and the currents can affect each other mutually. This leads to a nonlinear interaction process between waves and currents, and is demonstrated in Figure 5. Soulsby et al. (1993) devised a set of non-dimensional parameters for their parameterisation model: $y = \frac{\tau_m}{\tau_c+\tau_w}$, $Y = \frac{\tau_{max}}{\tau_c+\tau_w}$, where τ_c is the bed shear stress for the current-alone condition, and τ_w is the maximum bed shear stress within one wave cycle under wave-alone conditions. Both y and Y were plotted versus $x = \frac{\tau_c}{\tau_c+\tau_w}$, which typically represents the relative strengths of the current and the wave. Values of τ_c and τ_w were

determined directly using the input parameters U_{mean} and u_b: $\tau_c = \rho C_D {U_{mean}}^2$ and $\tau_w = 0.5\rho f_w {u_b}^2$, where C_D is the drag coefficient for the current U_{mean} on its own, f_w is the wave friction factor for an orbital velocity u_b on its own, and ρ is the density of water. In order to obtain a parameterised model for WCI, Soulsby et al. (1993) fitted one standard formula to all the models, with each model having its own set of fitting coefficients. The functions chosen give y and Y as functions of x, with a set of fitting coefficients determined by the nonlinear least-squares technique. As demonstrated by Soulsby et al. (1993), the angle between wave and currents (φ) has an influence on WCI. The strength of the nonlinear enhancement of both $y = \frac{\tau_m}{\tau_c+\tau_w}$ and $Y = \frac{\tau_{max}}{\tau_c+\tau_w}$ decreases with an increase in φ from 0° to 90°. These have been demonstrated by laboratory experiments, given in Section 3. Despite the good agreement between these models and experimental data, the basic physical processes and the fundamental mechanism of WCI cannot be fully described by the analytical approaches.

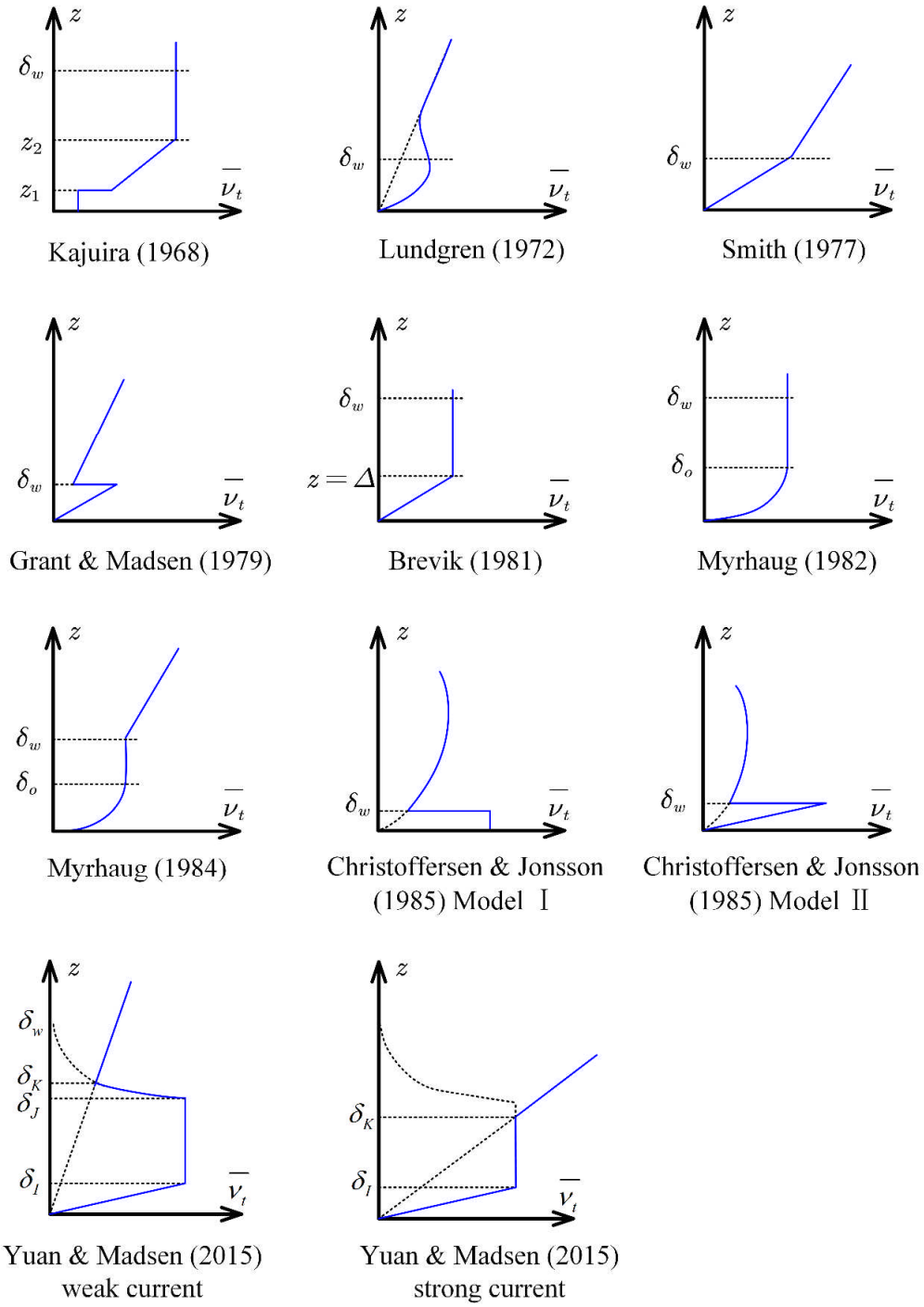

Figure 2. Eddy viscosity distributions for time-invariant WCI models, not to scale. (z_1 is the thickness of the viscous sublayer; z_2 is the upper limit of the overlap layer; δ_w is the thickness of the frictional layer for Kajuira, 1968 and the wave boundary layer thickness for the remainders; δ_0 is the thickness of the overlap layer; δ_I is the transition level: $\delta_I = 0.21\delta_w$; $\delta_J = 0.79\delta_w$; δ_K is where fourth-layer intersects the underlying three-layer structure; δ_w is the wave boundary layer thickness.)

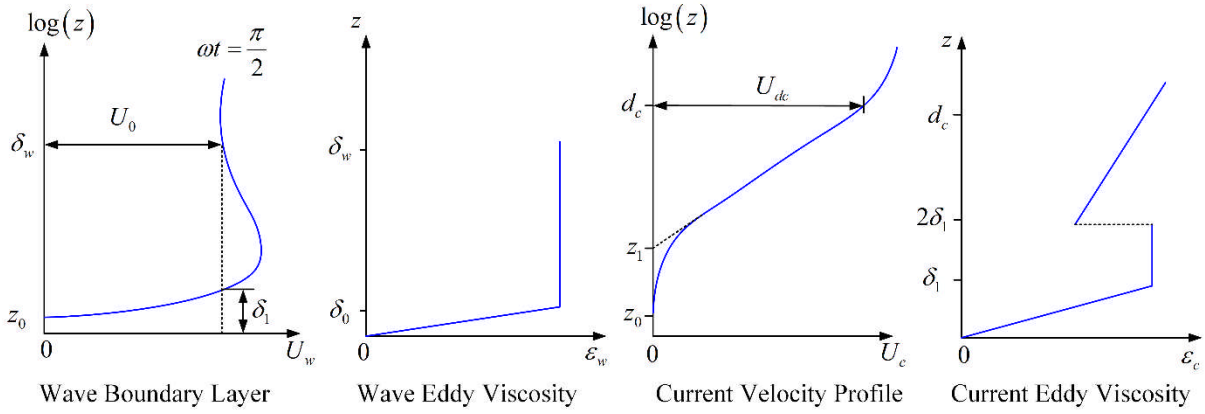

Figure 3. Eddy viscosity and velocity profiles for You et al. (1991). (z_0 is the elevation where the current velocity is zero; $z_1 = 2\delta_1[\frac{2.718\delta_1}{z_0}]^{-(U_C^*)/(U_{Cw}^*)}$; d_c is the elevation corresponding to the reference current velocity; $\delta_1 = \frac{0.5\kappa U_w^*}{\omega}$; $\delta_0 = 0.5\delta_1$; $\delta_w = \frac{4\kappa U_w^*}{\omega}$; U_w^* is the wave friction velocity under wave-alone condition.)

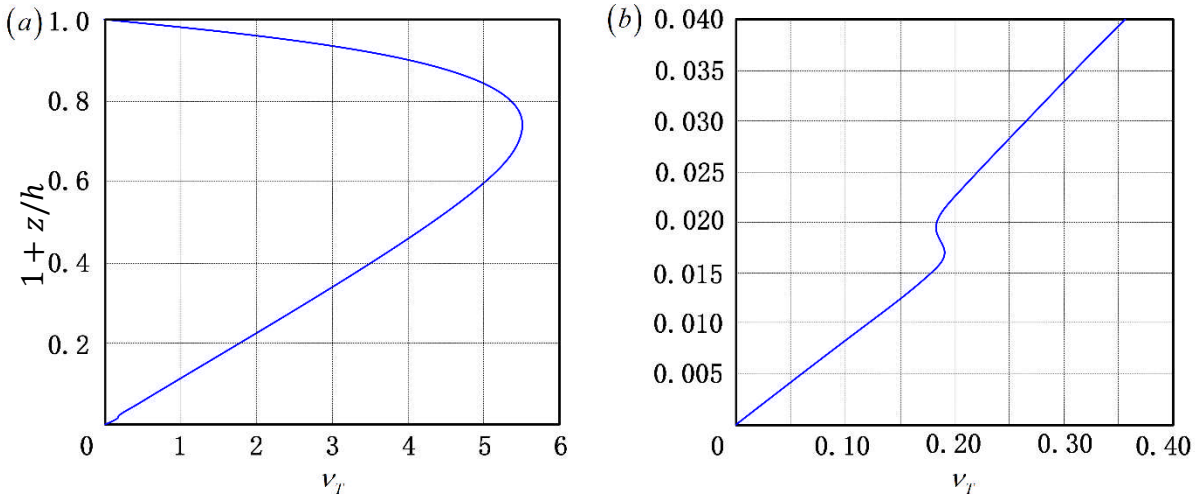

Figure 4. Eddy viscosity profile for Tambroni et al. (2015). (h is the dimensionless water depth; z is the dimensionless vertical displacement from the bed. ν_T is the dimensionless eddy viscosity.)

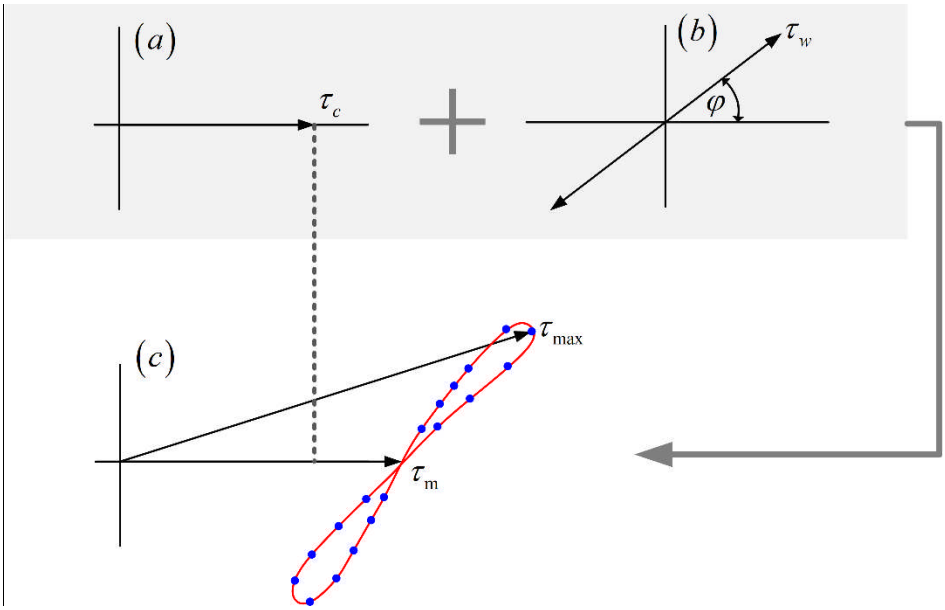

Figure 5. Schematic of bed shear-stresses in combined wave-current flows for Soulsby et al. (1993). (a) The current-alone stress; (b) the wave-alone stress, (c) the combined WCI stresses, having mean τ_m and maximum τ_{max}.

2.2 Numerical models

With the development of wave modelling, two main methods have been adopted to model wave generation and propagation: phase-solving models and phase-averaged models. Phase-solving models are based on vertically integrated, time-dependent mass and momentum balance equations. Phase-averaged models solve the energy or wave action balance equation. The first approach usually requires 10-100 time steps within one wave period and, therefore, is limited to relatively small-scale simulations. For large-scale applications, phase-averaged models are far more suitable.

2.2.1 Phase-solving models

The classical Boussinesq equations (Peregrine, 1967; Dingemans, 1997) are only applicable to a weak current condition. Many investigators have further developed the Boussinesq equations to be applicable to WCI. Yoon and Liu (1989) derived a set of Boussinesq equations, considering a much stronger current case. Chen et al. (1998) further developed the theory by considering the full dispersion terms. Zou et al. (2013) presented a new formulation of Boussinesq-type equations for wave-current interaction. Their work included the effect of current-induced mean water depth change on the wave motions.

Many investigators have used the wave board motion displacement for wave modelling in WCI. This is accomplished by prescribing velocity components based on the Stokes wave theory, and can be further categorised by the method of turbulence modelling for the current. With the development of Computational Fluid Dynamics (CFD), the Navier-Stokes equations can be solved by using numerical methods. There are three main approaches, namely, Direct Numerical Simulation (DNS), Unsteady Reynolds-Averaged Navier-Stokes (URANS) simulation, and Large Eddy Simulation (LES). DNS is a simulation solving the Navier–Stokes equations numerically without any turbulence model. Therefore, motions at all scales can be obtained from the results. LES is based on the principle that large eddies in a turbulent flow are mainly governed by geometry, while smaller eddies are more universal and independent of physical boundaries. This allows for computing the large three-dimensional turbulent structures directly from the Navier-Stokes equations and implicitly accounts for the

small eddies using a subgrid-scale (SGS) model. URANS simulation is based on the Unsteady RANS equations and can be further classified into Reynolds Stress Models (RSM), one-equation models, and two-equation models. One-equation models and two-equation models both rely on eddy viscosity assumptions, whereas RSM directly compute components of the Reynolds stress tensor using the Reynolds-stress transport equations, without relying on the eddy viscosity concept. Davies et al. (1988) adopted a one-equation turbulent energy closure to model the combined flow based on a linearised boundary layer equation and the assumption of parallel streamlines. Huynh-Thanh and Temperville (1991) developed a WCI model over rough beds, based on a simplified second-order $k - L$ turbulence model. Here, k represents the turbulent kinetic energy and L is the length scale. The model was further extended to oscillatory turbulent flow over rippled beds with some modifications. Holmedal et al. (2003) investigated the bottom wave-current boundary layer where random waves propagated with a turbulent current, using a high Reynolds number $k - \varepsilon$ turbulence model. Enhanced friction velocity and turbulent kinetic energy were found to be caused by the current. Yu et al. (2010) investigated the sediment transport beneath asymmetrical wavegroups, based on a $k - \varepsilon$ turbulence model modified for particle-laden flow (e.g. Hsu et al., 2004). Results suggest that for the grain diameter and high-velocity skewness wave condition, a nonlinear waveshape causes most onshore sediment transport. However, for those with relatively low wave skewness and a stronger offshore directed current, nonlinear boundary layer streaming may become the critical mechanism driving the net onshore transport. Teles et al. (2012; 2013) used a CFD approach (Code-Saturne) to investigate WCI and compared the results with the data of Klopman (1994) and Umeyama (2005). Both a two-equation and RSM turbulence closure methods were adopted in the model and the resulting velocity distributions showed good agreement with the reduction in the mean velocity near the free surface when waves were propagating with currents. However, the model was not fully capable of solving the bottom boundary layer, where a large discrepancy was found. This was ascribed by the authors to the wall function adopted in the model. The influence of the turbulence closure model on WCI was also investigated by Teles et al. (2012; 2013). Markus et al. (2013) adopted the CFD package Openfoam to model a combined wave and current condition, focusing on the evaluation of the flow field for a nonlinear wave combined with a nonuniform current. Zhang et al. (2014) used $k - \varepsilon$ turbulence modelling to study the effects of the wave period on the surface elevation and velocity distribution. The volume of fluid (VOF) method was applied to capture the free surface. Results showed that waves with a shorter period had a stronger interaction with the ambient current but had no effects on the bottom shear stress. Zhang et al. (2017) further developed the WCI model, by adopting the 'low Reynolds number modelling strategy' in the near-wall region. Details of bottom boundary layers were provided, such as time series of periodic velocities and bed shear stress. Due to its expensive computational costs, very few have applied the LES approach to model WCI over a smooth bed. Henn and Sykes (1999) adopted the LES approach to investigate fully developed turbulent flows over wave surfaces. Results indicated an increase in transverse velocity fluctuations on the wave upslope. This was found to be associated with temporally persistent vortex like structures located near the surface. Grigoriadis et al. (2012) investigated the effect of ripple steepness and relative current strength on turbulence characteristics of a combined flow, i.e. vorticity dynamics, turbulence statistics, bed shear stress, and pressure along the bed. Results indicated that larger bed forms in steeper ripples lead to stronger turbulence. Son and Lynett (2014) investigated the flow field under WCI, with an arbitrary angle between waves and currents. A set of depth-integrated equations was solved numerically, and the relative strength of wave radiation stress and bed shear stress was observed to represent the effect of turbulence induced by WCI.

A fundamentally different approach using DNS has also been applied to combined wave-current flows. Yang and Shen (2009) investigated coherent vortical structures (horseshoe vortices and streamwise vortices) in a turbulent Couette flow over a wavy surface. Results showed that vortical structures in the streamwise direction are dependent on the wave phase speed. The study was focused on kinematics near the free surface and is, therefore, applicable to wind-wave interaction. Guo and Shen (2013) investigated the effect of progressive gravity waves on isotropic turbulence in the underlying body of water. Waves considered in their model were 'rapid' and 'long'; i.e., the time scale of waves was much smaller than the turbulence, while the wavelength was much larger than the turbulence eddy size. They interpreted this as a common condition in the upper-ocean, and therefore, no discussion on the near-bottom flow field was given. Scandura (2007) investigated the steady streaming in a spatially uniform turbulent boundary layer generated by an oscillating pressure gradient using DNS. Results suggested the absence of steady streaming under a sinusoidal oscillating pressure gradient, and the presence of steady streaming in flows with a pressure gradient given by the sum of two sinusoidal functions. Blondeaux and Vittori (1994) studied the influence of wall imperfections on modifying the structure of the Stokes boundary layer using DNS. The wall waviness was assumed to be of small amplitude, and a high Reynolds number was considered. Results indicated that when the Reynolds number exceeded a critical value, an instant within the decelerating part of the cycle existed and unbounded perturbations of the flow in the Stokes layer were induced by a waviness of infinitesimal amplitude. Vittori and Verzicco (1998) studied the flow generated by an oscillating pressure gradient close to a wall with small imperfections, which were observed to play critical roles in triggering turbulence in the Stokes boundary layer. Costamagna et al. (2003) used DNS to investigate the dynamics of turbulent structures in the Stokes boundary layer when the flow departed from the laminar regime. Results of the velocity and vorticity fields indicated that the elementary process maintaining turbulence in oscillatory boundary layers is similar to that of steady flows. A sequence of events similar to those observed in steady boundary layers was observed, occurring periodically at approximately half the period of fluid oscillations. Mazzuoli et al. (2011) investigated the formation and dynamics of turbulent spots in an oscillatory boundary layer using DNS. The speeds of the head and tail of those spots were observed to scale with the instantaneous free stream velocity, similar to those found in steady turbulent boundary layers.

The issue of wave-induced streaming and its interaction with currents has been investigated by various authors. Holmedal and Myrhaug (2009) studied the seabed boundary layers beneath sinusoidal waves, Stokes second-order waves, and horizontally uniform boundary layers with asymmetric forcing. They highlighted two important mechanisms causing streaming, namely, turbulence asymmetry in successive wave half-cycles, and a vertical wave-induced velocity within the seabed boundary layer as originally explained by Longuet-Higgins (1953). Results suggested that the steady streaming in near-bed flows is induced by an interaction between the two mechanisms, depending on the degree of wave asymmetry and the ratio between wave lengths and the water depth. The Longuet-Higgins type streaming is always in the direction of wave propagation, while the turbulence-induced streaming is in the opposite direction. The asymmetry of second-order Stokes waves leads to a decrease of mass transport, so the wave-averaged Lagrangian velocity can be zero for waves with sufficiently long wavelength and large enough asymmetry for a particular water depth. Holmedal and Myrhaug (2013) further extended the work of Holmedal and Myrhaug (2009) by considering the existence of a following or an opposing current, providing new insights into the wave-current seabed boundary layers. Results showed that for waves following currents, the wave-averaged mean velocity is larger than that beneath horizontally uniform symmetric forcing and smaller than that in the current-alone condition. When waves propagate against the

currents, the value is smaller than that beneath horizontally uniform symmetric forcing and that in the current-alone condition. The net sediment transport was observed to be in the current direction for both following and opposing waves. Afzal et al. (2021) investigated the sediment transport due to wave-induced streaming under a nonzero angle between waves and currents. Results suggested that the mean sediment transport decreases with an increase in the angle between waves and currents. The mean sediment flux and bedload were both in the direction of wave propagation for the following (largest net sediment transport) and opposing (smallest net sediment transport) cases. For a fixed angle, the mean sediment transport was rotated towards the current from the wave propagation direction. Afzal et al. (2015) investigated the influence of three-dimensional wave-induced streaming on the seabed boundary layer, where waves propagate at an angle to the current. Veering of the mean velocity profiles was strongly affected by the streaming when waves and currents were not collinear. It was found that the influence of streaming weakened when the flow was more current-dominated. Fuhrman et al. (2009) adopted $k-\omega$ turbulence modelling systematically to compare the relative strengths of bed shear stresses and boundary layer streaming under wave motions from four contributions: i. converging-diverging effects from bed slope; ii. wave skewness; iii. wave asymmetry; iv. waves combined with superimposed negative currents, such as undertow and return currents. It was observed that wave skewness was the most important onshore contribution outside the surf zone. Fuhrman et al. (2013) used $k-\omega$ turbulence closure to simulate various boundary layer processes, including additional features: i. hindered settling velocities at high suspended sediment concentrations; ii. turbulence suppression induced by density gradients in the water–sand mixture; iii. boundary layer streaming caused by convective terms; and iv. converging–diverging effects due to a sloping bed. A validation over both hydraulically smooth and rough beds showed good performance of the model. It was found that for the medium-sized sand grains, streaming can enhance onshore sediment rates significantly. For fine sand, streaming can reverse the direction of net transport from offshore to onshore direction. Afzal et al. (2016) investigated sediment transport in the bottom boundary layer, where linear waves propagated at an angle with the current over various bottom roughnesses. Results suggested that the total sediment transport decreases with an increase in the roughness. The mean suspended sediment flux and bedload transport were observed to decrease when the angle between waves and currents increased.

2.2.2 Phase-averaged models

Phase-averaged models cannot provide detailed temporal information, but are generally appropriate for application to large areas of open oceans because of their less computational costs. Rusu and Soares (2011) adopted the SWAN model to investigate the effects of currents on the shape of the wave spectra. Results suggested that changes of the significant wave height induced by the currents can only be represented qualitatively. Quantitative agreement with the experimental data (see Section 3.1) can only be obtained by using a different current velocity. Guillou et al. (2016) studied the effects of waves on tidal kinetic energy in the Fromveur Strait. TOMAWAC was used for wave modelling, based on the wave action density equation. The important roles of bed shear stress were further confirmed. Results suggested that the enhanced bed shear stress induced by WCI, together with the wave radiation stress, reduced the tidal kinetic energy. This is demonstrated in Figure 6. Rapizo et al. (2017) adopted the SWAN model to investigate the energy dissipation induced by WCI. Results suggested that the model performs well when waves propagate with the current, but overestimates the wave height for the case of waves propagating against the current. The problem of overestimation was solved by a modification to enhance dissipation dependent on

the local current conditions. For more detailed information on the development of phase-averaged models, readers are referred to Roland and Ardhuin (2014).

Phase-averaged spectral wave models typically determine wave properties on the basis of linear theory for waves added to depth-uniform currents. However, currents in the real world are often sheared in the vertical direction. This leads to the necessity of treating the rotationality or shear in the flow field. Several studies have used a depth-weighted current to consider the influence of vertical current shear (Skop, 1987; Kirby and Chen, 1989). This has been used to calculate intrinsic frequency and action density in spectral wave models (van der Westhuysen and Lesser, 2007; Ardhuin et al., 2008). In application, this is further simplified by using only a weighted current based on the spectral peak wave number. This has been included as an option in widely used models such as Delft-3D and Coupled-Ocean-Atmospheric-Wave-Sediment Transport (COAWST) (Elias et al., 2012; Kumar et al., 2011, 2012). Kukulka et al. (2017) employed a spectral wave model to investigate typical wave characteristics in Delaware Bay and its adjacent coastal shelf. The model was based on a coupled application of the Regional Ocean Modelling System (ROMS) and Simulating WAves Nearshore (SWAN) within the COAWST modelling framework. Banihashemi et al. (2017) found that the depth-weighted current does not represent a consistent approximation for the current contribution to the group velocity at the leading order. Results demonstrated that using the weighted current as the current speed in the expression for absolute group velocity is inappropriate, and a corrected expression was derived. Banihashemi et al. (2019) investigated the differences in the wave action density and action flux caused by the current shear. Results were compared with those of Quinn et al. (2017), who determined the expressions for the wave action density and action flux in a similar way. It was found that the model of Banihashemi et al. (2019) was more accurate than Quinn et al. (2017). The proposed Taylor series expansion of the expressions for the wavenumber-dependent approximations about the reference value for the peak, as originally presented by Banihashemi et al. (2017), was extended by including the wave directionality and the variation in intrinsic frequency appearing in the denominator of the action density.

The numerical models established to date have provided various methods of generating waves and a turbulent current simultaneously, based on either two-dimensional or three-dimensional Navier-Stokes equations. See Appendices E to I for lists of the numerical methods and their key information. This is helpful when developing a combined condition numerically, though few of them include discussions on the underlying physical process. Research on the interaction between waves and vortices is limited to wind-wave interaction (Yang and Shen, 2009), and wave-current interaction near the free surface (Guo and Shen, 2013). Therefore, it calls for further studies of interaction between waves and vortices.

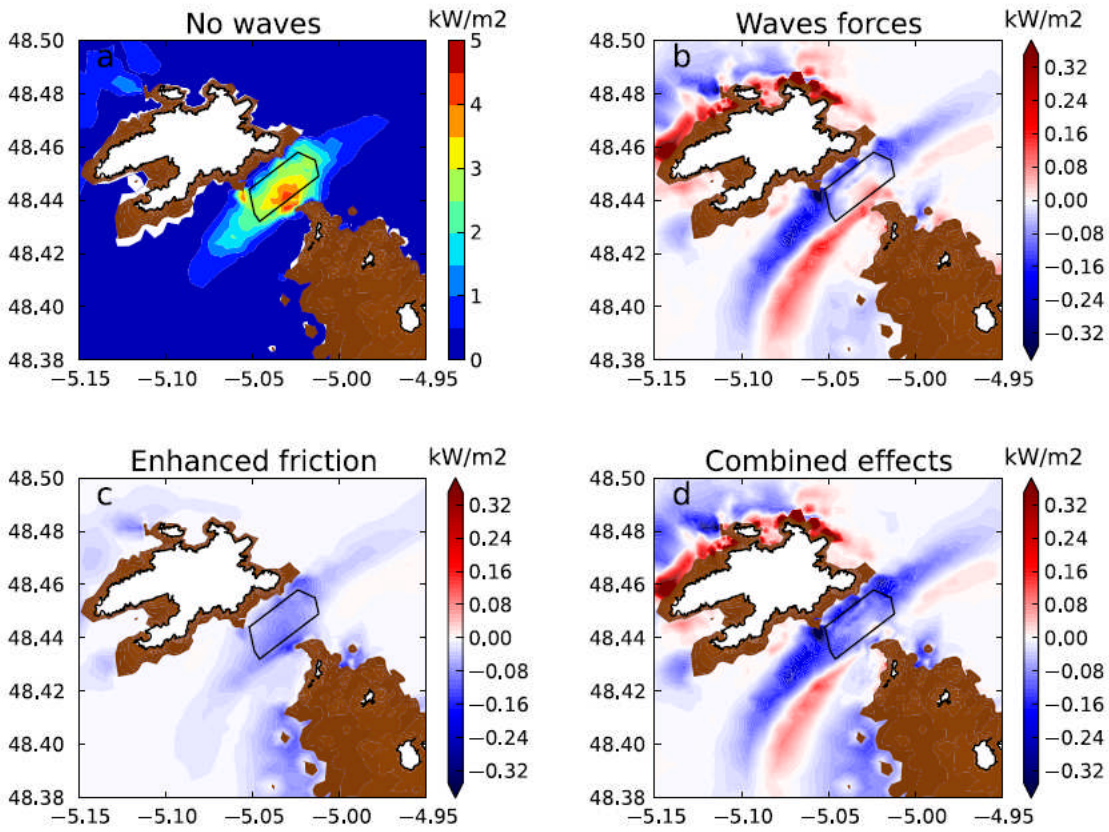

Figure 6. Averaged predicted tidal stream power 10 m above the bed during a neap-spring tidal cycle of March 1993 for configuration A: (a) Absolute values without waves. Relative differences with respect to predictions for: configurations with (b) waves forces, (c) enhanced bottom friction, and (d) combined effects. Predictions are shown for mean water depths over 20 m. Positive values suggest an increase of mean tidal stream power, while negative values indicate reduced kinetic energy. (After Guillou et al., 2016.)

2.3 Theories explaining WCI mechanism

Laboratory experiments, which will be reviewed in Section 3, have shown that the logarithmic mean velocity profile is altered when waves are superimposed onto a turbulent current. When waves are propagating with (against) the current, velocities increase (decrease) in the vicinity of the bed and decrease (increase) near the free surface. Since this cannot be fully explained by previous analytical models as discussed in the previous section, many theories have been developed to explain these changes. These can be divided into two main categories, one relying on wave-induced stresses and the other based on secondary circulations in laboratory facilities.

The first explanation relies on wave-induced Reynolds stress. When waves propagate with a current, negative wave-induced shear stress near the free surface results in decreased mean velocities. Figure 7 presents a schematic of the wave-induced Reynolds shear stress, together with the current-induced shear stress. Note that τ_0 is the current-induced bed shear stress, σ is the normal stress, and $\rho\widetilde{\widetilde{u}}\widetilde{\widetilde{w}}$ is the wave-induced Reynolds shear stress. When waves are propagating against the current, the current shear velocity is negative and has the same sign as the wave-induced Reynolds stress. Therefore, the presence of waves results in increased velocities near the free surface. Various expressions for wave-induced stress have been given by previous researchers. Nielsen and You (1996) derived expressions for wave-induced Reynolds stresses, based on the stress balance in the streamwise direction. The model is

mainly applicable to a wave-dominated condition, while a depth-dependent empirical factor is needed in the presence of a strong current. You (1996) proposed a semi-empirical 2D model, where the wave-induced second-order stress was a linear function of elevation and was dependent on the wave parameters, current magnitude, and the angle between waves and the current. Wave-induced stress at an arbitrary angle with the current was further investigated by Groeneweg and Klopman (1998) to achieve quantitative agreement with previous experiments, using the generalized Lagrangian mean approach.

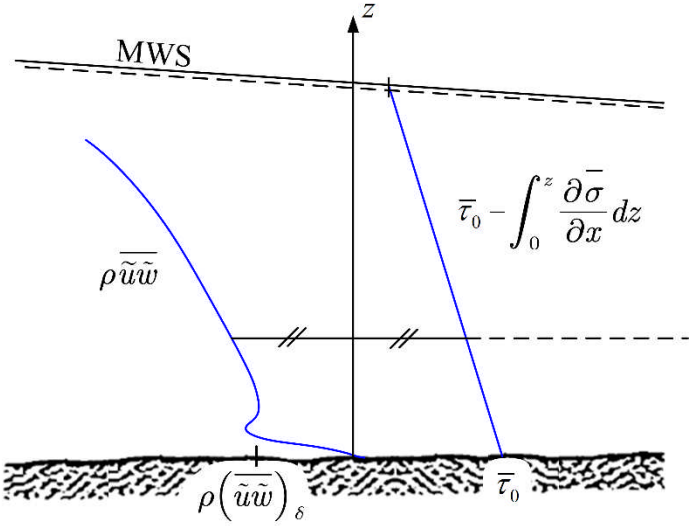

Figure 7. Shear stresses contributed from the currents and the waves for Nielsen and You (1996).

The other physical mechanism offering an explanation for changes in mean velocity profiles under WCI focusses on secondary circulations. Dingemans et al. (1996) presented a numerical model where secondary circulations, as predicted by the Craik-Leibovich (CL) vortex force theory (Craik and Leibovich, 1976), are responsible for the change in mean velocities near the free surface. The circulations consist of counter-rotating vortices with their axes in the streamwise direction, transporting low-momentum fluid near the side walls to the flume centre (see Figure 8 for a sketch). In the upper water column, the vortices cause a decrease in momentum and hence a decrease in mean velocities. Whereas in the lower water column, mean velocities are increased. Groeneweg and Battjes (2003) concluded that secondary circulations have a clear effect on the mean horizontal velocities, but this is relatively weak compared to the effect of streamwise driving forces. Numerical simulations also indicate that when the aspect ratio increases, the effects of secondary circulations become less obvious.

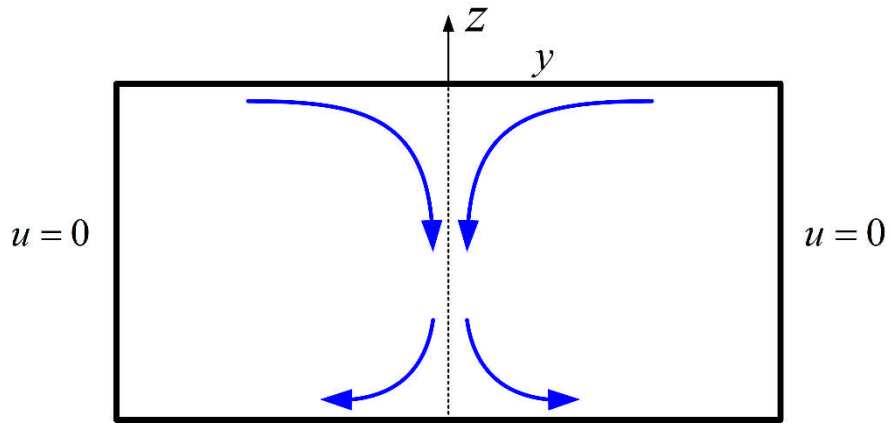

Figure 8. Circulations in a lateral vertical section for Dingemans et al. (1996).

More recently, other factors contributing to the changes in velocity profiles have been proposed such as flow non-uniformity along the flume. Yang et al. (2006) concluded that the momentum driven by secondary currents and/or non-uniformity caused by a free surface slope along the flume are contributing factors, in addition to wave-induced Reynolds stress. Olabarrieta et al. (2010) included the effects of variations in the wave-induced surface elevation. They concluded that velocity changes in the upper region were governed by wave-induced mass transport, while the flow region below the wave trough was dominated by wave-induced Reynolds stresses.

To conclude, existing theories involve either a local force balance in the streamwise direction or secondary circulations in a combined wave current flow. Qualitatively good agreements with previous data have been achieved, yet quantitatively good agreement depends on empirical factors adopted in most models.

3. Experiments

3.1 Laboratory experiments

Many researchers have investigated the changes in turbulent characteristics caused by the superimposition of waves, such as changes in the velocity profile and turbulent boundary layer thickness. Bakker and van Doorn (1978) performed laboratory experiments over a rough bed in a wave flume, where waves propagated with the current. Velocity distributions were obtained using laser-Doppler velocimetry (LDV) and compared with their theoretical solutions using the mixing length theory. Their results of mean and ensemble-averaged velocities showed good agreement with their theory, although a horizontally oscillating flow was assumed and is more applicable to oscillating water tunnel data. Brevik and Aas (1980) conducted experiments in a large-scale flume over a rippled bed. Their work was extended to the condition over a smooth bed by Brevik (1980). Velocities were measured using a micropropeller in both experiments and a decrease in mean velocity was observed in both conditions when waves propagated with the current.

A more comprehensive understanding of the velocity field and turbulence characteristics in combined wave-current flows was provided by Kemp and Simons (1982; 1983). Measurements using LDV indicated that the mean velocity profile remained logarithmic but with a reduction in velocities near the bed when waves propagated against the current. The mean velocities near the free surface were decreased (increased) when waves were propagating with (against) currents. Asano et al. (1986) conducted experiments in a wave tank over a rough bed, where waves propagated against the current. Results of mean velocity profiles suggested a similar trend to those observed by Kemp and Simons (1983), with a decrease in the lower region and an increase in the upper water column induced by the waves

superimposed. Klopman (1994) obtained similar results to Kemp and Simons (1982; 1983) for regular waves, and further investigated the effects of wave irregularity on the flow kinematics. LDV measurements showed less significant changes (but still qualitatively similar) in the mean velocities induced by random waves. Lodahl et al. (1998) conducted experiments in an oscillating water tunnel and obtained velocity measurements using LDV. Mean velocity distributions were observed to be logarithmic.

Umeyama (2005; 2009) used LDV to measure velocity components and Reynolds stress in the combined wave current case. Results showed that the difference between the mean velocities and the logarithmic profile was dependent on wave height and period. Flow reversals were also found near the bed in all the combined conditions tested, as indicated by the phase-averaged horizontal velocities. It was concluded that this had a retarding effect on the velocity profile. Particle image velocimetry (PIV) and particle tracking velocimetry (PTV) were used by Umeyama (2011) to obtain the instantaneous velocity fields and water particle trajectories. Periodic circulations composed of clockwise and anticlockwise vortices were observed for the wave-alone condition, but lost their shapes in the presence of the current. Yet, these circulations should be distinguished from the horseshoe vortices characterised in a turbulent boundary layer.

Singh and Debnath (2016) reported an experimental investigation of wave-current interaction in a laboratory flume. Velocities were measured by an Acoustic Doppler Velocimeter (ADV) to investigate the turbulence characteristics in a combined wave-current flow. The mean velocity profiles showed a decrease in the upper region and an increase near the bed, as previously observed by many researchers. However, their quadrant analysis results showed differences from the existing knowledge regarding turbulent boundary layers under current-alone conditions. There is a need for reliable experimental data to confirm quadrant contributions to Reynolds shear stress in a co-existing wave-current environment. Singh et al. (2016) studied the velocity field in a combined wave-current flow over a rough bed with three-dimensional roughness elements using ADV. Changes in the mean velocity profiles, Reynolds shear stress and turbulence intensities were investigated to quantify the influence of roughness spacing. This work was extended to the condition of a smooth bed by Singh et al. (2018a) using LDV for velocity measurements. Results of mean velocities again suggested a reduction near the free surface when waves were added. Similar flow patterns were observed over various bed configurations, i.e. an array of two hemispherical obstacles (Barman et al., 2016), a submerged hemisphere (Barman et al., 2017a), a pair of hemispherical obstacles (Barman et al., 2017b, 2018a), a rigid bed (Raushan et al., 2018), an array of cubical roughness (Singh et al., 2018b), 3D roughness composed of hemispheres (Barman et al., 2018b), and a cube (Singh et al., 2018c). Results showed that the scale of the recirculation zone decreased when waves were superimposed. The mean time intervals between ejections were observed to decrease in combined wave-current flows.

Previous experiments as reviewed above have demonstrated the profound changes in mean velocity profiles as induced by the superposition of waves. As reviewed in Section 2.3, secondary circulations are considered responsible for the changes in mean velocity observed when waves are added. In order to determine whether the predicted secondary flows occur, laboratory experiments have been performed by various researchers. For instance, Nepf and Monismith (1991) used LDA and visualisation beads near the free surface, showing that large-scale streamwise vortices only occur when waves are added; these became more obvious with increasing wave frequencies and wave heights. Klopman (1997) further examined the occurrence and strength of secondary flows, repeating the experiment of Klopman (1994) and carrying out measurements at different positions across the cross section. Both floater observations and LDV measurements proved the existence of secondary circulations as predicted by the CL-vortex force theory and previous numerical simulations.

An aspect ratio of 2 resulted in secondary circulations in all cases, including the 'current alone' case.

The flow kinematics in a combined flow, where waves propagate at right angles to the current, have been studied over various bed configurations. Sleath (1990a) examined the velocity field in a combined wave-current flow over smooth and rough boundaries, where waves were orthogonal to the turbulent current. An oscillating bed was used at the test section in a current flume to mimic combined wave-current boundary layers. This was similar to an oscillating water tunnel with a current at right angles. Velocities were measured using LDV and the mean velocity distributions were found to be qualitatively similar to the flow field where waves propagated with the current. This work was extended to the bed condition of ripples by Ranasoma and Sleath (1994). A logarithmic distribution was found to be valid in the outer region but not near the bed. This was explained by the formation and ejection of vortices close to the bed. Large-scale experiments were conducted by Simons et al. (1997) in the UK Coastal Research Facility. Velocities were measured by ADV and bed shear stresses were obtained by a shear cell. Results suggested an enhanced apparent bed roughness with the addition of relatively strong orthogonal waves, while the addition of a relatively weak longshore current had no such effect. Comparisons with various WCI models suggested that the models of Davies et al. (1988) and Fredsøe (1984) performed best. This set of data was later used for the validation of the model (Myrhaug et al., 2001), which was found to perform well for irregular waves in the amplitude to roughness ratio range of 20–200. The same facility was used further by MacIver and Simons (1997) to examine the refraction of waves by the currents. Fernando et al. (2011) conducted experiments in a wave tank (24 m long, 10 m wide, and 0.9 m deep). Velocities were measured by an ADV over rippled beds. Results indicated reduced near-bed velocities in the presence of orthogonal regular waves.

Lim and Madsen (2016) used ADV to measure the flow field over smooth and uniform rough beds. A linear interaction was observed for the smooth bed case. Results suggested an overestimation of the apparent roughness predicted by Grant and Madsen (1979), under a large angle of WCI. Faraci et al. (2018) carried out a thorough study of velocity distributions and turbulent fluctuations for orthogonal waves and currents over a bottom covered with different roughness elements. The experiments were conducted in a flume (18 m long, 4 m wide and 1.2 m deep). The velocity measurements were collected using a micro-Acoustic Doppler Velocimeter (ADV). Results showed that the probability density function of the total near-bed velocities can be represented by a Gaussian distribution for the current-alone case and a double-peaked distribution for the combined wave-current flows. Their experimental investigations provided new insights into the statistical properties of the near-bed velocity. Faraci et al. (2021) performed an extensive study of mean flow characteristics, velocity-inferred shear stresses and apparent roughness for orthogonal wave-current interaction over rough beds. A variety of flow conditions were tested, covering both wave dominated and current dominated regimes. Measurements of surface elevation and velocity profiles were obtained in the tank (35 m long, 25 m wide and 0.8 m deep) using wave gauges and Micro ADV. Observations showed that the superposition of waves increased the flow resistance when the combined flows were current-dominated. The opposite occurs when the flow is wave-dominated, irrespective of the bed roughness type. The apparent roughness was found to increase when the ratio of wave plus current to current only friction velocity increased.

The veering of currents has been observed in combined wave-current flows. Lim and Madsen (2016) performed an experimental study of periodic waves interacting with turbulent currents at 60°, 90° and 120° over smooth and uniform marble-covered rough beds. Mean velocities were measured using ADV in a wave-current basin (33 m long, 10 m wide and 0.9 m deep). Results showed an increase in the angle between the waves and the currents over the whole water depth, which is consistent with a wave-induced return flow superimposed on the

current. The veering of currents near the bed should be differentiated from that in the upper water column. This is attributed to the turbulence asymmetry induced by the current component in the direction of the near-bed wave orbital velocity which is shown to vary locally by ±10° due to disturbances generated at the inlet and outlet openings (referred to as "parasitic waves"). Faraci et al. (2018) found that the mean flow direction was modified as a consequence of the waves superimposed. For flows over a sandy bed roughness, results suggested very good agreement with those of Lim and Madsen (2016). The mean angle veered approximately -10° as a consequence of the wave-induced undertow current. However, the veering showed different features for flows over the gravel and rippled beds. In the vicinity of the bed, the current veered towards the beach up to 5° and then decreases up to −25° at the position 2 cm above the bed. This is caused by offshore directed streaming close to the bed, generated by the asymmetry in the wave shape and the large turbulent fluctuations induced by the large roughness that characterized these two cases.

WCI where waves propagate with currents at an arbitrary angle has been attempted over smooth and rough boundaries. Lim and Madsen (2016) found inaccuracies in determining apparent roughness for intersection angles of 60° and 120°. This was explained by the interference of logarithmic profiles, originating from wave-induced mass transport.

Bed shear stresses under combined waves and currents have also been studied because of their importance in sediment transport. Bakker and van Doorn (1978) were the first to obtain reliable experimental data of bed shear stresses when waves propagate following a current. Their results suggest that the bed shear stress obtained from the velocity measurements was in the same order of magnitude as that predicted by their theory. Brevik and Aas (1980) used experimental observations of wave attenuation to derive the friction factor in a combined wave-current flow. A rippled bed was adopted to reduce the relative effects from the smooth glass side walls. This is important because the results of Brevik (1980) were considered unsatisfactory because of significant sidewall effects. Kemp and Simons (1982) determined the bed shear stress from velocity measurements. Both logarithmic regions of the mean velocity profile and Reynolds shear stresses suggested an increase in bed shear stress when waves were superimposed. An increase in wave heights was observed to cause higher increments in the bed shear stress. Asano et al. (1986) used measurements of the mean water level gradient to deduce the bed friction. Results suggested an enhanced bed shear stress induced when waves were added. Sleath (1990a) determined the bed shear stress from velocity measurements. Results suggested reasonable agreement with the models of Grant and Madsen (1979) and Christoffersen and Jonsson (1985).

Lodahl et al. (1998) measured the bed shear stress using a hot-film probe in an oscillating water tunnel. Their results suggested that the time-averaged mean bed shear stress can increase, remain the same value, or decrease, in a combined wave-current flow. When the flow is current-dominated, bed shear stress remains unchanged by the waves (linear interaction between waves and currents). When the flow is wave-dominated and the wave boundary layer is in the laminar regime, bed shear stress decreases (nonlinear interaction). The decrease in the bed shear stress is ascribed to the phenomenon of re-laminarisation induced by the introduction of oscillatory motions. When the flow is wave-dominated and the wave boundary layer is turbulent, bed shear stress increases as commonly observed by previous researchers (nonlinear interaction). The aforementioned phenomenon of bed shear stress in WCI has also been observed when waves propagate with currents at a right angle (Musumeci et al., 2006; Faraci et al., 2021). Musumeci et al. (2006) performed experiments in a flume (18 m long, 4 m wide and 1.2 m deep) over beds with different bottom roughnesses. The flow structure for a regular wave interacting with currents was analysed using a micro ADV for velocity measurements. Results further confirmed that the phenomenon was also observed for the case of waves propagating with currents at a right

angle. Faraci et al. (2021) further studied the effects of WCI on the bed shear stress experimentally, enlarging the range of flow conditions in the literature. Results showed that for current-dominated flows, the flow resistance increased when waves were added. For flows in the wave-dominated regime with laminar wave boundary layers, the opposite occurred regardless of the bed roughness type. Simons and MacIver (2001) examined the bed friction for combined flows where waves propagated with and against a turbulent current. Results showed an enhancement of the mean bed shear stress and apparent bed roughness, induced by the addition of regular, bichromatic and random waves.

Simons et al. (2000) investigated the seabed friction, extending data from previous small scale and relative small orbital excursions to larger scale high Reynolds number oscillations in a large oscillating water tunnel. Measurements of the maximum shear stress for relatively strong currents were obtained. Direct measurements using LDV and a shear plate device indicated that the wave-induced friction factor was not sensitive to the current strength.

Ruessink et al. (2011) obtained measurements of instantaneous velocities, concentrations and fluxes in a large oscillating water tunnel. The experiments involved a range of flow conditions: two velocity-asymmetric flows, the same two flows propagating against a current, and a mixed skewed-asymmetric flow. Both well-sorted and medium-sized sand were considered in the experiments. Results suggest that the difference in magnitude of the fluxes between the two half cycles increases with an increase in velocity asymmetry and skewness. This leads to larger net transport rates, and is consistent with an increase in the skewness of the oscillatory bed shear stress, as observed from experiments.

Jepsen et al. (2012) made PIV measurements in a very small-scale flume (2 m long, 20 mm high, and 105.4 mm wide). The bed shear stress time history under various wave and current conditions was investigated and a considerable difference was observed between the Blasius solution and the PIV measurements, suggesting a change from laminar to turbulent flow as the flow reversed.

Bed shear stress when waves propagate orthogonally to the current has been investigated extensively. Simons et al. (1992) used a novel shear plate device to measure the mean and time-varying shear stresses directly, investigating the effects of nonlinear wave-current interaction on the mean and oscillatory velocity components within the bottom boundary layer. A significant change both in mean bed shear stress and apparent roughness were found when waves were added. This work was extended by Simons et al. (1994) from regular waves to random waves; it was found that random waves had a less significant effect on the mean flow. Arnskov et al. (1993) measured the instantaneous bed shear stress over a smooth bed. Both the magnitude and the direction of bed shear stress were obtained using a two-component hot-film probe. Results suggested that the mean bed shear stress was enhanced by the waves superimposed, whereas there was no non-linear enhancement of the maximum bed shear stress over a wave cycle. Fluctuations of bed shear stress were observed to decrease significantly when waves were added. Visser (1986) performed experiments in a wave basin. The bed friction was determined from the mean water level variation, similar to that adopted by Asano et al. (1986). An increase in bed shear stress was observed when waves were superimposed. The results of Klopman (1994), however, indicated that the addition of an orthogonal current had no obvious effect on the bottom friction. Ranasoma and Sleath (1994) investigated the bed condition of ripples, with the ripple crests parallel to the current and orthogonal to the waves. Values of shear velocity were determined from the velocity profiles and were well predicted by their model.

3.2 Field data

Field tests have been performed by many researchers to investigate the flow field in coastal boundary layers under the effects of WCI. It should be noted that field experiments in this

paper are only given a brief review. Black et al. (1996) performed field tests in the Bass Strait to examine the effects of WCI on the development of bed roughness and bed shear stress during storms. Observations suggested large roughness scales of 0.4 m and 0.067 m at water depths of 20 m and 40 m, respectively. Nayak et al. (2015) obtained velocity and bottom roughness measurements at a coastal ocean observatory off the New Jersey coast. Logarithmic velocity profiles were observed. The vertical component of the wave kinetic energy was increased within the roughness sublayer. Results of mixing lengths suggested agreement with the classical theories (Prandtl, 1925), regardless of flow conditions and bed roughness. Lewis et al. (2017) obtained ADCP measurements at two sites in the Irish Sea: i. 33.5 m water depth at Site A (53.4425°N and 4.2976°W), offshore of the port of Amlwch; ii. at Site B (53.3223°N and 4.7883°W), known locally as 'Holyhead Deep'. Mean velocity profiles followed a power law, while spatial and temporal variations of velocity were observed and explained by the interaction between waves and tidal currents. This finding was useful in the assessment of potential tidal energy sites, suggesting the importance of adopting a coupled wave-current model. The field observations carried out by Drost et al. (2018) within the northeastern region of the Australian North West Shelf further suggested the need to include nonlinear WCI in ocean circulation models. The observation sites were located in water depths of 40m and 74m between approximately 150 km and 230 km, respectively, northwest of Broome, Western Australia.

Field measurements of seabed shear stresses at two shallow sites (25 m depth in Cow Bay and 45 m depth on Sable Island Bank) on the continental shelf off Nova Scotia, Canada (Huntley and Hazen, 1988) have clearly identified the changes in kinematics and dynamics under a combined condition. Similar observations have been made near the seafloor in 18 m of water in the Strait of Juan de Fuca by Lambrakos et al. (1988), at a site (50° 35.82'N, 1° 31.51'W) in the English Channel 7.5 km south west of the coast of the Isle of Wight by Soulsby and Humphrey (1990), and at the Field Research Facility (FRF) in Duck, North Carolina by Trowbridge and Agrawal (1995). Cacchione and Drake (1979) performed field tests using the Geoprobe system in Norton Sound, Alaska. Simultaneous measurements of pressure and horizontal components of the current velocity were obtained at four levels. Wiberg and Smith (1983) further analysed the data of Cacchione and Drake (1979). Results suggest the importance of WCI on the continental shelf when estimating bed shear stresses. Results of the field tests conducted on the Northern California continental shelf between Point Arena and Point Reyes (Glenn, 1983; Grant and Glenn, 1983) suggest the same conclusion. Soulsby and Humphery (1990) obtained in situ measurements of velocities at a site in the English Channel. Results suggest that the presence of the wave boundary layer functioned as a source of turbulence to the current boundary layer. This leads to an increase in the turbulent kinetic energy and bed shear stress with the increasing wave/current ratio. See Figure 9 for an example. Note that E represents the turbulent kinetic energy, S_{40} is the mean velocity at z = 40cm, and σ_{wave} is the root-mean-square of the wave orbital velocity. Dalyander et al. (2013) used the field data obtained at the Middle Atlantic Bight (MAB), off the US East Coast (Lyne et al., 1990a, 1990b; Chang et al., 2001; Churchill et al., 1994). Lyne et al. (1990a, 1990b) collected data of stress and sediment transport at four sites in the Mid Atlantic Bight and on Georges Bank: i. at a water depth of 64 m on the southern flank of Georges Bank; ii. at a water depth of approximately 80 m on the west side of the Great South Channel; iii. at a water depth of 66 m at the eastern edge of a region of fine-grained sediments, referred to as the "Mud Patch"; iv. further southwest along the 60-m isobath in the Mid Atlantic Bight. Chang et al. (2001) obtained in-situ data at Mud Patch, located approximately 110 km south of Martha's Vineyard, Cape Cod, Massachusetts. The site is located on a broad continental shelf in the Mid Atlantic Bight in 70 m of water. Results suggest that sediment resuspension associated with hurricane Edouard was driven by the

effects of WCI. Both bed shear stress and dissipation rates in combined wave-current flows were observed to be increased with the passage of Hurricanes Edouard and Hortense. Churchill et al. (1994) measured data at four sand-dominated locations situated across the shelf in the Mid Atlantic Bight, with water depths ranging from 40 m to 130 m. Results indicate that good estimations of bed shear stress require accurate prediction of the wave energy spectrum. Zhu et al. (2016) obtained field data of water depths and near-bed velocities on an exposed tidal flat on the Eastern Chongming mudflat, located on the Yangtze River Delta, China. The data were used for an estimation of bed shear stress. Results suggest an overestimation of bed shear stress predicted by Grant and Madsen (1979) when the ratio of significant wave height to water depth is larger than 0.25. Their work also indicates the significance of winds on the estimation of bed shear stress under the combined wave-current condition. Soloviev et al. (2017) collected in-situ data in the Straits of Florida, using ADCP bottom moorings deployed on the Dania Beach shelf at the 11 m isobath (26.073°N, 80.101°W) and on the Miami Terrace at the 244 m isobath (26.191ºN, 79.974°W) and ship transects. Three forms of the Southward flow were observed, and were explained by the alongshore momentum balance with the alongshore pressure gradient. The value of the bottom drag coefficient was set due to the impact of WCI to solve the momentum balance equation.

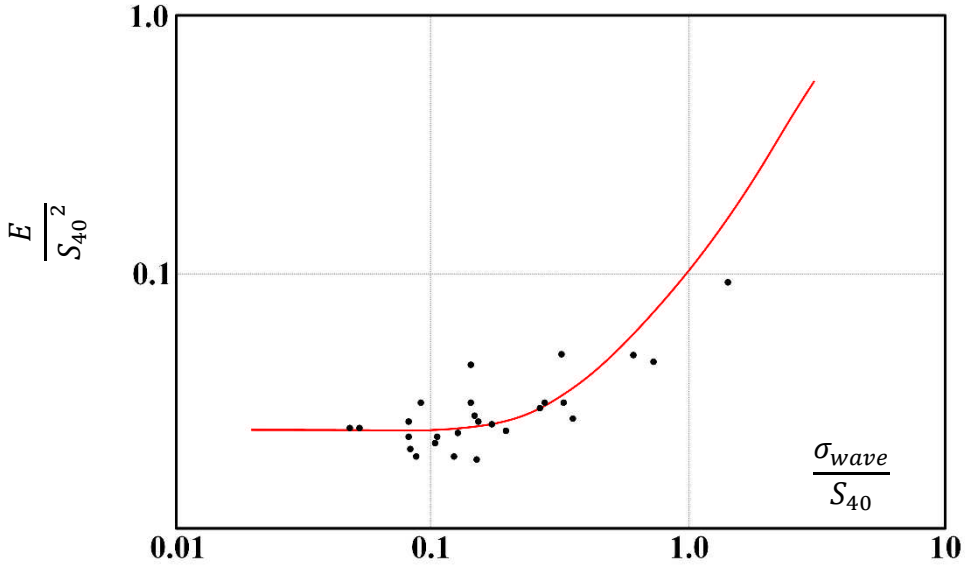

Figure 9. Normalised turbulent kinetic energy as a function of wave/current ratio for Soulsby and Humphery (1990).

Another important engineering application of WCI is in river mouths. When waves propagate with the tidal current, wave heights decrease. When waves propagate against the tidal current, wave heights increase and sometimes wave breaking can happen. Thomson et al. (2014) collected data of near-surface turbulence using freely drifting Surface Wave Instrument Floats with Tracking (SWIFTS) at the mouth of the Columbia River. Observations of the plume suggested the occurrence of breaking for short waves when encountering the currents at the edge of the plume. Much of this wave energy was converted to turbulence during the process of wave breaking. Zippel and Thomson (2017) collected measurements of waves and currents to evaluate wave breaking parameterizations in the same area. Results suggested that the effects of the sheared currents on the wavenumber spectrum are essential in calculating wave steepness accurately. Otherwise, an overestimation (underestimation) of wave steepness was observed by up to 20% for opposing (following) currents superimposed on waves.

The experiments discussed above cover a wide range of scales, from small flumes and large wave tanks to water tunnels and field conditions. Methods of wave generation and absorption, velocity measurements, and current generation have been described in the papers. For field conditions, an ocean current is a continuous and directed movement of sea water generated by a number of forces acting on the water, namely, wind, the Coriolis effect, breaking waves, and temperature and salinity differences. Therefore, various types of currents can be generated. Tidal currents occur with the rise and fall of the tides. The vertical movements of the tides near the shore cause the water to move horizontally, generating tidal currents. When a tidal current moves away from the sea, it 'floods'. When it moves towards the sea, it 'ebbs'. Surface oceanic currents are sometimes wind-driven. In the northern (southern) hemisphere, typical clockwise (anti-clockwise) rotations are developed by wind stresses. Deep oceanic currents are driven by differences in density and temperature. Turbulent boundary layers are generally fully developed and are similar to those in the laboratory. The turbulence characteristics are also similar if scaled correctly. Current velocity profiles are logarithmic and similar to those in the laboratory. However, it should be noted that field conditions are different from those in the laboratory. This is because the length and time scales of coastal wave boundary layers are significantly different from those of current boundary layers. For example, wave boundary layers are generally a few centimetres thick, while current boundary layers are typically a few metres thick. The time span of wave motions (i.e., wave period) is of the order of seconds, whereas the span of currents corresponds to the tidal frequency. Another significant difference is the flow pattern near the seabed. This is mainly caused by bed roughness conditions. Appendices J and K summarise test methodologies for laboratory experiments and field tests, respectively.

4. Conclusions

4.1 The present

Based on this comprehensive review of previous studies on WCI, the main conclusions from a technical point of view are as follows:

i. Changes of wave characteristics (i.e., wave lengths and wave heights) induced by WCI are well predicted by existing models;
ii. Experimental data from laboratory experiments are mainly for shorter waves, with a limited range of wave periods tested;
iii. There is still a lack of *in situ* data to validate mean velocities and wave kinematics.

From a physical point of view, the main conclusions are listed:

i. Many studies have observed an enhanced mean bed shear stress induced by WCI; however, the mean bed shear stress can also be decreased or unaltered when waves are superimposed on currents. This phenomenon has been observed in laboratory studies (e.g. Lodahl et al., 1998; Musumeci et al., 2006; Faraci et al., 2021) and is of importance to coastal engineers and researchers~~;~~. These different types of bed shear stress behaviours with the addition of waves are explained by the type of WCI: the unchanged mean bed shear stress is caused by the linear interaction between waves and currents; the decreased bed shear stress is explained by the flow re-laminarisation of oscillatory motions; and the enhanced bed shear stress is caused by the nonlinear interaction between waves and currents.
ii. Mean velocities are increased near the bed and decreased in the upper water column when a current propagates with the waves; this phenomenon is explained by wave-induced stresses (Nielsen and You, 1996; You, 1996; Groeneweg and Klopman, 1998), secondary circulations in laboratory facilities (Dingemans et al., 1996;

Groeneweg and Battjes, 2003), flow non-uniformity along the flume (Yang et al., 2006) and wave-induced mass transport (Olabarrieta et al., 2010).

iii. For wave and currents which are not collinear, the mean flow can experience changes not only in the magnitude but also in the direction of flow. The veering of a current over depth has been observed to be induced by the superposition of waves (Lim and Madsen, 2016; Faraci et al., 2018) and is explained by the superposition of wave-induced flow on the nominal current, steady streaming induced by momentum transfer (Longuet-Higgins, 1953), and turbulence asymmetry (Trowbridge and Madsen, 1984; Yuan and Madsen, 2015) within the wave boundary layer;

iv. Most existing algebraic models are based on an eddy viscosity assumption. Various assumed distributions have been proposed and these have been shown to describe velocities reasonably well for near-bed regions; however, validation in the outer region is less convincing;

v. Numerical models have been found to predict the phenomenon (as stated in ii) with acceptable accuracy, mainly based on URANS models; however, validation of the models is limited to some tests and not performed using a wide range of experimental data. They produce accurate results in the near-bed region but velocities further from the bed are less well predicted;

vi. Future studies can develop an enhanced understanding of WCI in all three-dimensions. Turbulent boundary layers are composed of many vortices varying in scale, which are not necessarily confined to a two-dimensional plane. The full three-dimensional velocity flow field in WCI is necessary for the understanding of lateral dispersion. In light of the significance of turbulent vortices to transport processes, an enhanced understanding of three-dimensional turbulence characteristics under the effects of waves is essential for an accurate description of coastal environment.

4.2 The future

Despite the significant progress in the study of WCI through mathematical and experimental approaches, the field is still challenging and lacks knowledge in many perspectives.

Many eddy viscosity profiles have been proposed to relate the mean velocity field with Reynolds shear stress, but very few of them have been validated against a full range of experimental data. This calls for future studies of experiments which can be used for validation. Note that the sensitivity of eddy viscosity distributions to the mean velocity and Reynolds shear stress in a combined wave-current flow is also unknown, which should be addressed in the future.

When dealing with wave-induced Reynolds shear stress, there is still a lack of a comprehensive database for validation. Existing models are based on some empirical factors which have been obtained from the limited amount of experimental data. This calls for systematic investigations in the future.

In the framework of both numerical and experimental studies, Reynolds numbers covered are still far too low. It remains unclear whether the existing theory of WCI can be upscaled to real ocean environment. Therefore, it is suggested that large-scale controlled experiments would be useful for future investigations of WCI. This would facilitate the testing of models without the problem of scaling and experimentally-imposed boundary constraints. The direct solution of the N-S equations at high Reynolds number will become possible as computer processing power grows. Although there is very restricted usage of LES and DNS for numerical modelling of WCI, we envision a bright future for these two approaches.

From a physical point of view, existing theories of WCI are mainly focused on collinear/orthogonal waves and currents. It is suggested that future studies build on the work

of Faraci et al. (2021) and provide a better insight to cases where the waves and currents intersect at arbitrary angles. Considering that ocean waves are random waves, it is recommended that an enhanced understanding of nonlinear waves interacting with turbulent currents from an academic perspective would be helpful for coastal engineers. Remaining challenges also exist in the interaction between waves and currents over various forms of seabed, such as over a fixed rippled bed. This calls for future studies of field tests and theoretical models.

Acknowledgments

The authors gratefully appreciate for the financial support from the UCL Dean's Prize and the China Scholarship Council (CSC). This work was supported by the National Natural Science Foundation of China (Grant No. 51909074, 51879096), China Postdoctoral Science Foundation (Grant No. 2019M661713), the Fundamental Research Funds for the Central Universities (B210202024), and Key Laboratory of Coastal Disaster and Defence of Ministry of Education, Hohai University (Grant No. 201912).

Appendix A – Keyword index of bibliography on eddy viscosity-based models

1. Bed configuration

- Smooth beds

Myrhaug and Slaattelid (1990), Christoffersen and Jonsson (1985), Tambroni et al. (2015)

- Transitional beds

Myrhaug and Slaattelid (1990), Christoffersen and Jonsson (1985)

- Rough beds

Lundgren (1972), Grant and Madsen (1979), Myrhaug and Slaattelid (1990), Malarkey and Davies (1998) for ($a/k_s > 30$), Yuan and Madsen (2015), Myrhaug (1982), Christoffersen and Jonsson (1985), Myrhaug and Slaattelid (1989), You et al. (1991), You (1994a), You (1994b), Tambroni et al. (2015)

2. Eddy viscosity temporal distribution

- Time-invariant

Lundgren (1972), Grant and Madsen (1979), Myrhaug and Slaattelid (1990), Yuan and Madsen (2015), Myrhaug (1982), Christoffersen and Jonsson (1985), Myrhaug and Slaattelid (1989), You et al. (1991), You et al. (1992), You (1994a), You (1994b), Tambroni et al. (2015)

- Time-dependent

Malarkey and Davies (1998)

3. Eddy viscosity spatial distribution

- Two-layer

Lundgren (1972), Grant and Madsen (1979), Myrhaug and Slaattelid (1990), Malarkey and Davies (1998), Myrhaug (1982), Christoffersen and Jonsson (1985), You et al. (1991) for the wave-induced eddy viscosity, You et al. (1992), You (1994b) for the wave-induced eddy viscosity, Tambroni et al. (2015)

- Three-layer

Yuan and Madsen (2015) for the case of a strong current, Myrhaug and Slaattelid (1989), You et al. (1991) for the current-induced eddy viscosity, You (1994a), You (1994b) for the current-induced eddy viscosity

- Four-layer

Yuan and Madsen (2015) for the case of a weak current

4. Independent/Dependent between wave and current eddy viscosity

- Independent

Lundgren (1972), You et al. (1991), You (1994b)

- Dependent

Grant and Madsen (1979), Myrhaug and Slaattelid (1990), Malarkey and Davies (1998), Yuan and Madsen (2015), Christoffersen and Jonsson (1985), Myrhaug and Slaattelid (1989), You (1994a), Tambroni et al. (2015)

5. Experimental data used for model validation

- Jonsson (1963)

Lundgren (1972) for the wave-induced eddy viscosity

- Jonsson and Carlsen (1976)

Malarkey and Davies (1998) for the wave-only case, Myrhaug (1982), You et al. (1991) in the bottom boundary layers, You et al. (1992) in the bottom boundary layers, You (1994b)

- Bakker and Van Doorn (1978)

Myrhaug and Slaattelid (1990) in the bottom boundary layers, Christoffersen and Jonsson (1985) for friction velocities, Myrhaug and Slaattelid (1989) in the bottom boundary layers

- Jonsson (1980)

Myrhaug (1982)

- Van Doorn (1981)

You et al. (1991) in the bottom boundary layers, You (1994a) in the bottom boundary layer, You (1994b): unsatisfactory in near-bed regions, Myrhaug and Slaattelid (1990) in the bottom boundary layers, Myrhaug and Slaattelid (1989) in the bottom boundary layers

- Van Doorn (1982)

You et al. (1991) in the bottom boundary layers, You et al. (1992) in the bottom boundary layers, You (1994b): unsatisfactory in near-bed regions

- Kemp and Simons (1982)

Grant and Madsen (1979), Myrhaug and Slaattelid (1990) in the bottom boundary layers, Christoffersen and Jonsson (1985) for friction velocities, You (1994b) in the bottom boundary layer, Tambroni et al. (2015)

- Coffey (1987)

You (1994a) in the bottom boundary layer

- Myrhaug et al. (1987)

Myrhaug and Slaattelid (1990) in the bottom boundary layers, Myrhaug and Slaattelid (1989) in the bottom boundary layers

- Lambrakos et al. (1988)

Myrhaug and Slaattelid (1989) in the bottom boundary layers

- Jensen (1989)

You et al. (1991) in the bottom boundary layers, You (1994b)

- Soulsby and Humphery (1990)

Myrhaug and Slaattelid (1990) in the bottom boundary layers

- Klopman (1994)

Tambroni et al. (2015)

- Umeyama (2005)

Tambroni et al. (2015)

- Yuan and Madsen (2015)

Grant and Madsen (1979), Yuan and Madsen (2015): good agreements in some test conditions, but significant discrepancies found in other test conditions

Appendix B – Keyword index of bibliography on mixing length models

1. Bed configuration

- Smooth bed

Umeyama (2005, 2009)

2. Experimental data used for model validation

Umeyama (2005, 2009) for velocity distributions

Appendix C – Keyword index of bibliography on momentum-integral-method model (Fredsøe, 1984)

1. Bed configuration

- Smooth and Rough bed

Fredsøe (1984)

2. Experimental data used for model validation

Bakker and van Doorn (1978), Simons et al. (1997) for friction factors

Appendix D – Keyword index of bibliography on parameterised models

1. Bed configuration

- Rough bed

Soulsby et al. (1993), Holmedal et al. (2000)

2. Experimental data used for model validation

Extensive data available from laboratory experiments and field tests

3. Main outcomes

Bed shear stress

Appendix E – Keyword index of bibliography on one-equation models (Davies et al., 1988)

1. Bed configuration

- Rough bed

2. Experimental data used for model validation

- None

3. Main outcomes

- Velocity, turbulent energy k, shear stress, and eddy viscosity distributions

4. Determination of eddy viscosity

- Obtained by the numerical results of k, with mixing length scale l being specified as a function of k ($\varepsilon_t = c_0 \cdot l \cdot \sqrt{k}$).

Appendix F – Keyword index of bibliography on two-equation models

1. Bed configuration

- Smooth bed

Fuhrman et al. (2009), Fuhrman et al. (2013), Teles et al. (2012, 2013), Zhang et al. (2014), Zhang et al. (2017)

- Rough bed

Huynh-Thanh and Temperville (1991), Holmedal et al. (2003), Holmedal and Myrhaug (2009), Fuhrman et al. (2009), Yu et al. (2010), Holmedal and Myrhaug (2013), Fuhrman et al. (2013), Teles et al. (2012, 2013), Afzal et al. (2015), Afzal et al. (2016), Afzal et al. (2021).

- Rippled bed

Huynh-Thanh and Temperville (1991)

2. Main outcomes

- Mean velocity profiles

Huynh-Thanh and Temperville (1991), Holmedal et al. (2003), Holmedal and Myrhaug (2009), Fuhrman et al. (2009), Yu et al. (2010), Holmedal and Myrhaug (2013), Fuhrman et al. (2013), Teles et al. (2012, 2013), Afzal et al. (2015), Zhang et al. (2017)

- Ensemble-averaged velocities

Huynh-Thanh and Temperville (1991), Holmedal et al. (2003), Zhang et al. (2014), Zhang et al. (2017)

- Time-averaged turbulence quantities

Huynh-Thanh and Temperville (1991)

- Turbulent kinetic energy

Holmedal et al. (2003)

- Shear stresses within bottom boundary layers

Holmedal et al. (2003), Holmedal and Myrhaug (2009), Fuhrman et al. (2009), Holmedal and Myrhaug (2013), Fuhrman et al. (2013), Afzal et al. (2021)

- Mean concentration profiles

Yu et al. (2010), Fuhrman et al. (2013), Afzal et al. (2021)

- Net sediment transport rate

Yu et al. (2010), Fuhrman et al. (2013)

- Time series of sediment concentrations

Holmedal and Myrhaug (2009)

- Wave-averaged sediment flux profiles

Holmedal and Myrhaug (2009), Holmedal and Myrhaug (2013), Fuhrman et al. (2013), Afzal et al. (2021), Afzal et al. (2016).

- Time series of sediment flux profiles

Fuhrman et al. (2013)

3. Turbulence models

- k-L model

Huynh-Thanh and Temperville (1991)

- k-ε model

Holmedal et al. (2003), Holmedal and Myrhaug (2009), Holmedal and Myrhaug (2013), Yu et al. (2010), Teles et al. (2012, 2013), Zhang et al. (2014), Zhang et al. (2017), Afzal et al. (2021), Afzal et al. (2015), Afzal et al. (2016).

- k-ω model

Fuhrman et al. (2009), Fuhrman et al. (2013), Teles et al. (2012, 2013)

4. Determination of eddy viscosity

- Obtained from the numerical results of k and mixing length scale L:

$$\varepsilon_t = \sqrt{2k} \cdot L/4$$

Huynh-Thanh and Temperville (1991)

- Obtained from the numerical results of k, and the turbulent dissipation rate ε:

$$\varepsilon_t = c_1 \cdot k^2/\varepsilon$$

Holmedal et al. (2003), Holmedal and Myrhaug (2009), Holmedal and Myrhaug (2013), Afzal et al. (2021), Afzal et al. (2015), Afzal et al. (2016).

- Obtained from the numerical results of k, and the turbulent dissipation rate ε:

$$\varepsilon_t = c_\mu \cdot k^2(1 - ø)/\varepsilon$$

Yu et al. (2010)

- Obtained from the numerical results of k, and the specific dissipation rate ω:

$$\varepsilon_t = k/\max(\omega, \frac{7}{8} \cdot \frac{\left|\frac{\partial u}{\partial y}\right|}{\sqrt{0.09}})$$

Fuhrman et al. (2013)

5. Experimental data used for model validation

- Van Doorn (1981)

Huynh-Thanh and Temperville (1991) for the case condition 'V20RA' over flat rough beds in the bottom boundary layer region (lower than 4.5cm), Holmedal et al. (2003) for the case condition 'V20RA' under WCI in the bottom boundary layer region (lower than 6cm).

- Kemp and Simons (1982)

Zhang et al. (2017) for the case condition 'WCA1', limited numbers of comparisons.
Holmedal and Myrhaug (2013) for the mean bottom boundary layer velocities.

- Sumer et al. (1986)

Huynh-Thanh and Temperville (1991) for the wave-only case over flat rough beds in the bottom boundary layer region (lower than 4.5cm).

- Sleath (1990a)

Holmedal et al. (2003) for mean velocity profile under WCI in the bottom boundary layer region (lower than 3cm).

- Justesen (1991)

Holmedal et al. (2003) for regular waves-alone case.

- Klopman (1994)

Teles et al. (2012, 2013): unsatisfactory in the near-bed region (from the bed to 0.3cm above) and mean velocities were overestimated from 0.3cm to 1cm.
Holmedal and Myrhaug (2013) for the mean bottom boundary layer velocities.

- Umeyama (2005)

Teles et al. (2012, 2013): good agreements found in some test conditions and mean velocities were underestimated in some other conditions.
Holmedal and Myrhaug (2013) for the mean bottom boundary layer velocities.

- Umeyama (2011)

Zhang et al. (2014): discrepancies found, especially in the test condition 'WC1', only three test conditions were compared.

- Dohmen-Janssen and Hanes (2005)

Yu et al. (2010)

- Dohmen-Janssen et al. (2001)

Afzal et al. (2021) for the wave-averaged suspended sediment concentration profiles.

- Dohmen-Janssen and Hanes (2002)

Fuhrman et al. (2013) and Afzal et al. (2021) for the wave-averaged sediment transport.

- Yuan and Madsen (2015)

Afzal et al. (2015) for the mean velocity profiles.

- Sumer et al. (1993)

Fuhrman et al. (2013) for the mean velocity profiles.

- O'Donoghue and Wright (2004b)

Fuhrman et al. (2013) for the instantaneous sediment flux profiles.

- Hassan and Ribberink (2005)

Fuhrman et al. (2013) for the sediment transport rate.

Appendix G – Keyword index of bibliography on RSM (Teles et al., 2012, 2013)

1. Bed configuration

- Smooth and Rough bed

2. Experimental data used for model validation

- Klopman (1994): not accurate for predicting Reynolds shear stress;
- Umeyama (2005): large discrepancies found.

3. Main outcomes

- Mean velocity profiles
- Reynolds shear stress
- Eddy viscosity profiles

4. Determination of eddy viscosity

- Obtained from the RSM model directly, using the numerical results of test conditions from Umeyama (2005).
- A tentative parameterised model for eddy viscosity under WCI was further given, but lacks accuracy and also needs more experimental data for validations.

Appendix H – Keyword index of bibliography on LES models

1. Bed configuration

- Rippled bed

Grigoriadis et al. (2012)

- Rough bed

Son and Lynett (2014)

- Tidal energy stream site

Guillou et al. (2016)

- Smooth bed

Henn and Sykes (1999)

2. Main outcomes

- Size and location of the recirculation regions

Grigoriadis et al. (2012)

- Vorticity dynamics of the separated flows

Grigoriadis et al. (2012)

- Statistical characteristics of turbulence

Henn and Sykes (1999), Grigoriadis et al. (2012)

- Bed shear stress

Henn and Sykes (1999), Grigoriadis et al. (2012)

- Mean velocity profiles & Time series of velocities

Henn and Sykes (1999), Son and Lynett (2014)

- Wave heights

Son and Lynett (2014), Guillou et al. (2016)

- Peak wave period

Guillou et al. (2016)

- Mean wave direction

Guillou et al. (2016)

- Current amplitude and direction

Guillou et al. (2016)

- Kinetic energy

Guillou et al. (2016)

3. Eddy viscosity models used for SGS models

- Ducros et al. (1996)

Grigoriadis et al. (2012)

- Smagorinsky (1963)

Son and Lynett (2014), Guillou et al. (2016)

4. Experimental data used for model validation

- Fredsøe et al. (1999)

Grigoriadis et al. (2012)

- Kemp and Simons (1982, 1983)

Son and Lynett (2014)

- Swan (1990)

Son and Lynett (2014)

- Guillou et al. (2016)

Guillou et al. (2016)

- Buckles et al. (1984)

Henn and Sykes (1999)

Appendix I – Keyword index of bibliography on DNS models

1. Bed configuration

- Smooth bed (wavy surface)

Yang and Shen (2009), Blondeaux and Vittori (1994), Vittori and Verzicco (1998), Costamagna et al. (2003), Mazzuoli et al. (2011)

- Smooth bed (flat surface)

Guo and Shen (2013), Scandura (2007)

2. Main outcomes

- Velocity field

Vittori & Verzicco (1998), Costamagna et al. (2003), Scandura (2007), Yang and Shen (2009), Mazzuoli et al. (2011), Guo and Shen (2013)

- Vorticity magnitude and directions

Vittori & Verzicco (1998), Costamagna et al. (2003), Scandura (2007), Yang and Shen (2009), Guo and Shen (2013)

- Vorticity evolutions

Yang and Shen (2009), Guo and Shen (2013), Costamagna et al. (2003)

- Reynolds stress

Scandura (2007), Yang and Shen (2009), Guo and Shen (2013)

- Surface shear stress and pressure

Yang and Shen (2009)

- Correlation of coherent vortices with scalar mixing and friction drag at the wave surface

Yang and Shen (2009)

- Turbulence velocity spectrum

Guo and Shen (2013), Costamagna et al. (2003)

- Stream function

Blondeaux and Vittori (1994)

- Turbulent kinetic energy

Vittori & Verzicco (1998), Mazzuoli et al. (2011)

- Turbulence intensities

Vittori & Verzicco (1998)

- Wall shear stress

Vittori & Verzicco (1998), Costamagna et al. (2003), Scandura (2007), Mazzuoli et al. (2011)

3. Experimental data used for model validation

- Carstensen et al. (2010)

Mazzuoli et al. (2011)

Appendix J – Keyword index of bibliography on laboratory experiments

1. Bed configuration

- Smooth bed

Brevik (1980), Thomas (1981), Kemp and Simons (1982, 1983), Visser (1986), Sleath (1990a), Thomas (1990), Swan (1990), Nepf and Monismith (1991), Arnskov et al. (1993), MacIver and Simons (1997), Lodahl et al. (1998), Simons and MacIver (2001), Umeyama (2005), Musumeci et al. (2006), Umeyama (2009), Jepsen et al. (2012), Umeyama (2011), Rusu and Soares (2011), Yuan and Madsen (2015), Singh and Debnath (2016), Lim and Madsen (2016)

- Rough bed

Bakker and von Doorn (1978) for $\frac{a}{k_s} = 3 \sim 4$, Kemp and Simons (1982, 1983), Asano et al. (1986), Visser (1986), Sleath (1990a), Simons et al. (1992), Simons et al. (1994), Klopman (1994), Klopman (1997), Simons et al. (1997), Simons et al. (2000) for $\frac{a}{k_s} = 7 \sim 70$ and $\frac{a}{k_s} \leq 5$, Simons and MacIver (2001) for $\frac{a}{k_s} = 0.02 \sim 1.25$, Musumeci et al. (2006), Fernando et al. (2011), Ruessink et al. (2011), Yuan and Madsen (2015), Lim and Madsen (2016), Singh et al. (2016), Singh et al. (2018a), Barman et al. (2016), Barman et al. (2017a), Barman et al. (2017b, 2018a), Raushan et al. (2018), Singh et al. (2018b), Barman et al. (2018b), Singh et al. (2018c), Faraci et al. (2018), Faraci et al. (2021).

- Rippled bed

Brevik and Aas (1980), Ranasoma and Sleath (1994), Fredsøe et al. (1999) for $\frac{a}{k_s} \approx 1$, Faraci et al. (2018).

2. Main outcomes

- Mean velocity profiles

Bakker and von Doorn (1978), Brevik (1980), Brevik and Aas (1980), Kemp and Simons (1982, 1983), Swan (1990), Nepf and Monismith (1991), Ranasoma and Sleath (1994), Klopman (1994), Klopman (1997), Simons et al. (1997), MacIver and Simons (1997), Lodahl et al. (1998), Fredsøe et al. (1999), Simons et al. (2000), Simons and MacIver (2001), Umeyama (2005), Musumeci et al. (2006), Umeyama (2009), Fernando et al. (2011), Yuan and Madsen (2015), Lim and Madsen (2016), Singh and Debnath (2016), Singh et al. (2016), Singh et al. (2018a), Barman et al. (2016), Barman et al. (2017a), Barman et al. (2017b), Barman et al. (2018a), Singh et al. (2018b), Barman et al. (2018b), Singh et al. (2018c), Faraci et al. (2021)

- Bed shear stress and/or apparent roughness

Bakker and von Doorn (1978), Brevik (1980), Brevik and Aas (1980), Kemp and Simons (1982, 1983), Visser (1986), Simons et al. (1992), Arnskov et al. (1993), Simons et al. (1994), Simons et al. (1997), Lodahl et al. (1998), Simons et al. (2000), Simons and MacIver (2001), Fernando et al. (2011), Ruessink et al. (2011), Jepsen et al. (2012), Yuan and Madsen (2015), Lim and Madsen (2016), Faraci et al. (2021)

- Velocity profiles under the wave crest and wave trough

Thomas (1981), Kemp and Simons (1982, 1983), Sleath (1990a), Thomas (1990), Swan (1990), Simons et al. (1997), Ruessink et al. (2011), Faraci et al. (2018)

- Instantaneous velocity fields (vectors)

Umeyama (2011), Ruessink et al. (2011), Faraci et al. (2018)

- Turbulent fluctuations

Kemp and Simons (1982, 1983), Klopman (1997), Fredsøe et al. (1999), Umeyama (2005), Umeyama (2009), Barman et al. (2016), Barman et al. (2017a), Barman et al. (2017b), Barman et al. (2018a), Raushan et al. (2018), Singh et al. (2018b), Barman et al. (2018b), Singh et al. (2018c)

- Skewness and flatness of turbulent fluctuations

Faraci et al. (2018)

- Reynolds shear stress

Kemp and Simons (1982, 1983), Klopman (1997), Umeyama (2005), Umeyama (2009), Singh and Debnath (2016), Singh et al. (2016), Singh et al. (2018a), Barman et al. (2016), Barman et al. (2017a), Barman et al. (2017b), Faraci et al. (2018), Singh et al. (2018b), Barman et al. (2018b)

- Turbulence intensities

Kemp and Simons (1982, 1983), Singh and Debnath (2016), Singh et al. (2016), Barman et al. (2016), Barman et al. (2017b), Barman et al. (2018b), Singh et al. (2018c)

- Reynolds shear stress contributed from four quadrant events

Singh and Debnath (2016), Barman et al. (2016), Barman et al. (2017a), Barman et al. (2017b), Barman et al. (2018b)

- Probability density function of the stream-wise velocity fluctuations

Faraci et al. (2018), Barman et al. (2018b)

- Probability density function of the streamwise velocities

Faraci et al. (2018)

- Joint probability distribution of turbulence fluctuations

Singh et al. (2018a)

- Power spectra of velocities

Klopman (1997), Barman et al. (2016), Barman et al. (2017a), Barman et al. (2018a), Barman et al. (2018b), Singh et al. (2018c)

- Turbulence production

Barman et al. (2017a), Raushan et al. (2018), Singh et al. (2018b)

- Turbulence kinetic energy

Barman et al. (2017a), Barman et al. (2018a), Raushan et al. (2018), Singh et al. (2018b), Singh et al. (2018c)

- Pressure energy diffusion

Raushan et al. (2018)

- Turbulent energy dissipation

Raushan et al. (2018), Singh et al. (2018b)

- Turbulent energy diffusion

Raushan et al. (2018)

- Skewness of velocity fluctuations

Barman et al. (2017a), Singh et al. (2018c)

- Eddy viscosity & mixing length

Barman et al. (2018a)

- Mean water level gradient

Asano et al. (1986)

- Wavelengths and wave heights

Thomas (1981), Kemp and Simons (1982, 1983), Thomas (1990), Faraci et al. (2021)

- Wave direction

MacIver and Simons (1997)

- Mean flow direction

Faraci et al. (2018), Faraci et al. (2021)

- Ripple development

Fernando et al. (2011)

- Wave spectrum

Rusu and Soares (2011)

- Motions of surface beads

Nepf and Monismith (1991)

- Concentration profiles

Ruessink et al. (2011)

- Sand fluxes

Ruessink et al. (2011)

- Erosion depths

Ruessink et al. (2011)

3. Facility type

- Wave flumes

Bakker and von Doorn (1978), Brevik (1980), Brevik and Aas (1980), Thomas (1981), Kemp and Simons (1982, 1983), Asano et al. (1986), Sleath (1990a), Thomas (1990), Swan (1990), Nepf and Monismith (1991), Ranasoma and Sleath (1994), Klopman (1994), Klopman (1997), Fredsøe et al. (1999), Simons and MacIver (2001), Umeyama (2005), Umeyama (2009), Jepsen et al. (2012), Umeyama (2011), Singh and Debnath (2016), Singh et al. (2016, 2018a, 2018b, 2018c), Barman et al. (2016, 2017a, 2017b, 2018a, 2018b), Raushan et al. (2018), Faraci et al. (2018);

- Wave basins

Visser (1986), Simons et al. (1992), Arnskov et al. (1993), Simons et al. (1994), Simons et al. (1997), MacIver and Simons (1997), Musumeci et al. (2006), Fernando et al. (2011), Rusu and Soares (2011), Lim and Madsen (2016), Faraci et al. (2021);

- Oscillating water tunnels

Lodahl et al. (1998), Simons et al. (2000), Ruessink et al. (2011), Yuan and Madsen (2015);

4. Instrument for velocity measurements

- Micropropeller

Brevik (1980), Brevik and Aas (1980), Visser (1986)

- Hot-film probe

Arnskov et al. (1993)

- ADV

Simons et al. (1992), Simons et al. (1994), Simons et al. (1997), MacIver and Simons (1997), Musumeci et al. (2006), Fernando et al. (2011), Lim and Madsen (2016), Singh and Debnath (2016), Singh et al. (2016, 2018a, 2018b, 2018c), Barman et al. (2016, 2017a, 2017b, 2018a, 2018b), Raushan et al. (2018)

- Micro-ADV

Faraci et al. (2018), Faraci et al. (2021)

- Electromagnetic Current Meter (EMCM) and Acoustic Doppler Velocimeter Profiler (ADVP)

Ruessink et al. (2011)

- LDV

Bakker and von Doorn (1978), Thomas (1981), Kemp and Simons (1982, 1983), Visser (1986), Sleath (1990a), Thomas (1990), Swan (1990), Nepf and Monismith (1991), Ranasoma and Sleath (1994), Klopman (1994), Klopman (1997), Lodahl et al. (1998), Fredsøe et al. (1999), Simons et al. (2000), Simons and MacIver (2001), Umeyama (2005), Umeyama (2009)

- PIV

Jepsen et al. (2012), Umeyama (2011), Yuan and Madsen (2015)

- PTV

Umeyama (2011)

5. Wave Conditions

- Fixed Wave period T

Bakker and von Doorn (1978), Thomas (1981), Kemp and Simons (1982, 1983), Thomas (1990), Klopman (1994), Klopman (1997), Fredsøe et al. (1999), Fernando et al. (2011), Umeyama (2011);

- Fixed Wave height H

Bakker and von Doorn (1978), Sleath (1990a), Thomas (1990), Klopman (1997), Simons et al. (1997), MacIver and Simons (1997), Fredsøe et al. (1999), Lim and Madsen (2016), Singh et al. (2018a);

- Varying wave periods and wave heights

Brevik (1980), Brevik and Aas (1980), Asano et al. (1986), Visser (1986), Simons et al. (1992), Swan (1990), Nepf and Monismith (1991), Arnskov et al. (1993), Ranasoma and Sleath (1994), Simons et al. (1994), Simons et al. (1997), Lodahl et al. (1998), Simons and MacIver (2001), Umeyama (2005), Musumeci et al. (2006), Umeyama (2009), Jepsen et al. (2012), Rusu and Soares (2011), Yuan and Madsen (2015), Singh and Debnath (2016), Singh et al. (2016, 2018b, 2018c); Barman et al. (2016, 2017a, 2017b, 2018a, 2018b), Raushan et al. (2018), Faraci et al. (2018), Faraci et al. (2021).

6. Eddy viscosity distributions

- Given in the near-bed region

Kemp and Simons (1982, 1983): $y \leq 35mm$.

- Given throughout the whole water depth

Singh et al. (2018a): Non-dimensional eddy viscosity, using shear velocity and water depth as scaling parameters.

Appendix K – Keyword index of bibliography on field tests

1. Main outcomes

- Bed shear stress

Huntley and Hazen (1988), Glenn (1983), Grant and Glenn (1983), Lambrakos et al. (1988), Soulsby and Humphrey (1990), Black et al. (1996), Nayak et al. (2015), Zhu et al. (2016), Lewis et al. (2017), Drost et al. (2018)

- Bed roughness

Black et al. (1996), Nayak et al. (2015), Lewis et al. (2017), Drost et al. (2018)

- Pressure

Cacchione and Drake (1979), Soloviev et al. (2017)

- Velocities

Cacchione and Drake (1979), Lambrakos et al. (1988), Trowbridge and Agrawal (1995), Black et al. (1996), Thomson et al. (2014), Nayak et al. (2015), Guillou et al. (2016), Zhu et al. (2016), Lewis et al. (2017), Zippel and Thomson (2017), Drost et al. (2018)

- Wave height and/or wavelength

Black et al. (1996), Thomson et al. (2014), Nayak et al. (2015), Hashemi et al. (2016), Guillou et al. (2016), Lewis et al. (2017), Zippel and Thomson (2017)

- Reynolds shear stresses

Nayak et al. (2015), Zhu et al. (2016)

- Spectra of velocities

Nayak et al. (2015), Zhu et al. (2016), Lewis et al. (2017)

- Mixing Length & Eddy Viscosity

Nayak et al. (2015)

- Turbulence kinetic energy: Production, and Dissipation Rates

Thomson et al. (2014), Nayak et al. (2015), Guillou et al. (2016), Zhu et al. (2016)

- Wave breaking rate

Zippel and Thomson (2017)

2. Site

- Norton Sound, Alaska

Cacchione and Drake (1979)

- Northern California

Glenn (1983), Grant and Glenn (1983)

- Nova Scotia

Huntley and Hazen (1988)

- Strait of Juan de Fuca

Lambrakos et al. (1988)

- 7.5 km southwest of the coast of the Isle of Wight

Soulsby and Humphrey (1990)

- Duck, North Caroline

Trowbridge and Agrawal (1995)

- Bass Strait

Black et al. (1996)

- Middle Atlantic Bight (MAB)

Dalyander et al. (2013)

- Mouth of the Columbia River

Thomson et al. (2014), Zippel and Thomson (2017)
- New Jersey coast

Nayak et al. (2015)
- Pentland Firth and Bristol Channel

Hashemi et al. (2016)
- Fromveur Strait (ADCP site)

Guillou et al. (2016)
- Yangtze River Delta, China

Zhu et al. (2016)
- Irish Sea, UK

Lewis et al. (2017)
- Straits of Florida

Soloviev et al. (2017)
- Australian North West Shelf

Drost et al. (2018)

3. Instrument
- Suspended sediment monitors and a video camera

Black et al. (1996)
- Electromagnetic flowmeters

Huntley and Hazen (1988), Lambrakos et al. (1988), Soulsby and Humphrey (1990), Black et al. (1996)
- LDV

Trowbridge and Agrawal (1995)
- Surface Wave Instrument Floats with Tracking (SWIFTS)

Thomson et al. (2014), Zippel and Thomson (2017)
- ADV

Nayak et al. (2015)
- PIV

Nayak et al. (2015)
- ADCP

Soloviev et al. (2017), Guillou et al. (2016), Lewis et al. (2017)
- Doppler profilers

Zippel and Thomson (2017)
- Aquadopp current profilers

Drost et al. (2018)
- Wave buoys

Hashemi et al. (2016), Guillou et al. (2016), Drost et al. (2018)
- Geoprobe system

Cacchione and Drake (1979)
- Ship transects

Soloviev et al. (2017)

4. Assessment of theoretical models used for predicting bed shear stress/wave properties
- Grant and Madsen (1979)

Huntley and Hazen (1988) found good agreement. Trowbridge and Agrawal (1995) found good agreement for seabed flow structures. Nayak et al. (2015) did not observe the outer log-layer in mean velocity profiles as predicted by the model; results suggested 20%-80% overestimation of friction velocity by the model. Drost et al. (2018) found reasonable

agreement when predicting the enhancement of apparent bottom roughness; however, observations during the most wave-dominated conditions suggested over-prediction by the model.

- Myrhaug and Slaattelid (1989)

Lambrakos et al. (1988) found fair agreement.

- Myrhaug and Slaattelid (1990)

Soulsby and Humphrey (1990) found good agreement.

- Hashemi et al. (2016)

Hashemi et al. (2016) found reasonable agreement for the two field sites.

References

[1] Afzal, M.S., Holmedal, L.E. and Myrhaug, D., 2015. Three-dimensional streaming in the seabed boundary layer beneath propagating waves with an angle of attack on the current. Journal of geophysical research: Oceans, vol. 120, no. 6, pp. 4370-4391.

[2] Afzal, M.S., Holmedal, L.E., Myrhaug, D., 2016. Effect of bottom roughness on sediment transport due to streaming beneath linear propagating waves with an angle of attack on current. Scour and Erosion: Proceedings of the 8th International Conference on Scour.

[3] Afzal, M.S., Holmedal, L.E. and Myrhaug, D. 2021. Sediment Transport in Combined Wave–Current Seabed Boundary Layers due to Streaming. Journal of hydraulic engineering, vol. 147, no. 4.

[4] Aiki, H. and Greatbatch, R.J., 2012. Thickness-weighted mean theory for the effect of surface gravity waves on mean flows in the upper ocean. Journal of Physical Oceanography, 42(5), pp.725-747.

[5] Aiki, H. and Greatbatch, R.J., 2013. The vertical structure of the surface wave radiation stress for circulation over a sloping bottom as given by thickness-weighted-mean theory. Journal of Physical Oceanography, 43(1), pp.149-164.

[6] Akan, C., Moghimi, S., Ozkan-Haller, H. T., Osborne, J. and Kurapov, A., 2017. On the dynamics of the Mouth of the Columbia River: Results from a three-dimensional fully coupled wave-current interaction model. J. Geophys. Res. Oceans, 122, 5218–5236.

[7] Ardhuin, F., Jenkins, A.D. and Belibassakis, K.A., 2008. Comments on “The three-dimensional current and surface wave equations”. Journal of Physical Oceanography, 38(6), pp.1340-1350.

[8] Ardhuin, F., Rascle, N., Belibassakis, K.A., 2008. Explicit wave-averaged primitive equations using a generalized Lagrangian mean. Ocean Model, 20, 35–60.

[9] Arnskov, M.M., Fredsøe, J. and Sumer, B.M., 1993. Bed shear stress measurements over a smooth bed in three-dimensional wave-current motion. Coastal Engineering, 20(3-4), 277-316.

[10] Asano, T., Nakagawa, M. and Iwagaki, Y., 1986. Changes in current properties due to wave superimposing. In Coastal Engineering 1986, 924-939.

[11] Bakker, W., and van Doorn, T., 1978. Near-bottom velocities in waves with a current. Proc. 16th Coastal Engng. Conf., Hamborg, ASCE, chapter 82, 1394-1413.

[12] Banihashemi, S., Kirby, J.T. and Dong, Z. 2017. Approximation of wave action flux velocity in strongly sheared mean flows. Ocean modelling, vol. 116, pp. 33-47.

[13] Banihashemi, S. and Kirby, J.T., 2019. Approximation of wave action conservation in vertically sheared mean flows. Ocean modelling, vol. 143, pp. 101460.

[14] Barman, K., Debnath, K. and Mazumder, B.S., 2016. Turbulence between two inline hemispherical obstacles under wave–current interactions. Advances in Water Resources, 88, 32-52.

[15] Barman, K., Debnath, K. and Mazumder, B.S., 2017a. Higher-order turbulence statistics of wave–current flow over a submerged hemisphere. Fluid Dynamics Research, 49(2), 025504.
[16] Barman, K., Debnath, K. and Mazumder, B.S., 2017b. Turbulence study over submerged obstacles on waves and currents combined flow. ISH Journal of Hydraulic Engineering, 23(3), 246-257.
[17] Barman, K., Debnath, K. and Mazumder, B.S., 2018a. Turbulence over a pair of submerged hemispheres in presence of surface waves and following current. Journal of Offshore Mechanics and Arctic Engineering, 140(3), 031104.
[18] Barman, K., Roy, S. and Debnath, K., 2018b. Wave-current generated turbulence over hemisphere bottom roughness. Estuarine, Coastal and Shelf Science, 202, 1-17.
[19] Bennis, A.C. and Ardhuin, F., 2011. Comments on "The depth-dependent current and wave interaction equations: a revision". Journal of Physical Oceanography, 41(10), pp.2008-2012.
[20] Black, K., Rosenberg, M., Symonds, G., Simons, R., Pattiaratchi, C. and Nielsen, P., 1996. Measurements of the wave, current and sea level dynamics of an exposed coastal site. Mixing in Estuaries and Coastal Seas, 50, 29-58.
[21] Blondeaux, P. and Vittori, G., 1994. Wall imperfections as a triggering mechanism for Stokes-layer transition. J. Fluid Mech., 264, 107–135.
[22] Boussinesq, J., 1877. Essai sur la théorie des eaux courantes, Mémoires présentés par divers savants à l'Académie des Sciences, 23(1), 1-680.
[23] Brevik, I., 1980. Flume experiment on waves and currents II. Smooth bed. Coastal Engineering, 4, 89-110.
[24] Brevik, I., 1981. Oscillatory rough turbulent boundary layers. J. Waterway, Port, Coastal and Ocean Eng. Div., ASCE, 107(WW3): 175-188.
[25] Brevik, I. and Aas, B., 1980. Flume experiment on waves and currents. I. Rippled bed. Coastal Engineering, 3, 149-177.
[26] Buckles, J., Hanratty, T. J. and Adrian, R. J., 1984. Turbulent flow over large-amplitude wavy surfaces. J. Fluid Mech., 140, 27-44.
[27] Cacchione, D. A. and Drake, D. E., 1979. A new instrument system to investigate sediment dynamics on continental shelves. Marine Geology, 30, 299-312.
[28] Carstensen, S., Sumer, B. M. and Fredsøe, J., 2010. Coherent structures in wave boundary layers. Part 1. Oscillatory motion. J. Fluid Mech. 646, 169–206.
[29] Chang, G.C., Dickey, T.D., Williams III, A.J., 2001. Sediment resuspension over a continental shelf during Hurricanes Edouard and Hortense. Journal of Geo- physical Research 106, 9517–9531.
[30] Chen, Q., Madsen, P.A., Schäffer, H.A., and Basco, D.R., 1998. Wave-current interaction based on an enhanced Boussinesq approach, Coastal Eng., 33, 11–39.
[31] Christoffersen, J.B. and Jonsson, I.G., 1985. Bed friction and dissipation in a combined current and wave motion. Ocean Engineering, 12, 387-423.
[32] Churchill, J.H., Wirick, C.D., Flagg, C.N., Pietrafesa, L.J., 1994. Sediment resuspension over the continental shelf east of the Delmarva Peninsula. Deep Sea Research Part II: Topical Studies in Oceanography 41, 341–363.
[33] Clark, T., Roc, T., Fisher, S. and Minns, N., 2015. Turbulence and turbulent effects in turbine and array engineering. A guide for the tidal power industry. Tech. Rep. MRCF-TiME-KS10.
[34] Coffey, F.C., 1987. Current profiles in the presence of waves and the hydraulic roughness of natural sand beaches. Ph.D. thesis, Dept. of Geography, University of Sydney.

[35] Costamagna, P., Vittori, G. and Blondeaux, P., 2003. Coherent structures in oscillatory boundary layers. J. Fluid Mech., 474, 1–33.
[36] Craik, A.D.D. and Leibovich, S., 1976. A rational model for Langmuir circulations. J. Fluid Mech., 73(3), pp. 401-426.
[37] Dalyander, P.S., Butman, B., Sherwood, C.R., Signell, R.P. and Wilkin, J.L., 2013. Characterizing wave-and current-induced bottom shear stress: US middle Atlantic continental shelf. Continental Shelf Research, 52, pp.73-86.
[38] Davies, A.G., Soulsby, R.L., and King, H.L., 1988. A numerical model of the combined wave and current bottom boundary layer. Journal of Geophysical Research, 93, 491-508.
[39] Dingemans, M. W., Kester, J.A.Th.M.V., Radder, A.C. and Uittenbogaard, R.E., 1996. The effect of the CL-vortex force in 3D wave-current interaction. In Proc. 25th Intl Conf. on Coastal Engng, Orlando, chapter 375, 4821–4832.
[40] Dingemans, M.W., 1997. Water Wave Propagation over Uneven Bottoms, Part 2 – Nonlinear Wave Propagation, Singapore, World Scientific, 13, 473–967.
[41] Dohmen-Janssen, C. M., and Hanes, D. M., 2005. Sheet flow and suspended sediment due to wave groups in a large wave flume. Cont. Shelf Res., 25, 333– 347.
[42] Dohmen-Janssen, C. M., Hassan, W. N. and Ribberink, J. S., 2001. Mobile-bed effects in oscillatory sheet flow. J. Geophys. Res. Oceans, 106 (C11): 27103–27115.
[43] Dohmen-Janssen, C. M., and Hanes, D. M., 2002. Sheet flow dynamics under monochromatic nonbreaking waves. J. Geophys. Res. Oceans, 107 (C10): 13–21.
[44] Drost, E.J., Lowe, R.J., Ivey, G.N. and Jones, N.L., 2018. Wave-current interactions in the continental shelf bottom boundary layer of the Australian North West Shelf during tropical cyclone conditions. Continental Shelf Research, 165, 78-92.
[45] Ducros, F.D., Comte, P.C., Lesieur, M., 1996. Large-eddy simulation of transition to turbulence in a boundary layer developing spatially over a flat plate. Journal of Fluid Mechanics, 326, 1-36.
[46] Elias, E.P.L., Gelfenbaum, G., Van der Westhuysen, A.J., 2012. Validation of a coupled wave-flow model in a high-energy setting: The mouth of the Columbia River. J. Geophys. Res. 117, C09011.
[47] Faraci, C., Scandura, P., Musumeci, R. E., and Foti, E., 2018. Waves plus currents crossing at a right angle: near-bed velocity statistics. Journal of Hydraulic Research, 56(4), 464-481.
[48] Faraci, C., Musumeci, R. E., Marino, M., Ruggeri, A., Carlo, L., Jensen, B., Foti, E., Barbaro, G., and Elsaßer, B., 2021. Wave-and current-dominated combined orthogonal flows over fixed rough beds. Continental Shelf Research, 220, 104403.
[49] Fernando, P.C., Guo, J.K., and Lin, P.Z., 2011. Wave–current interaction at an angle 1: experiment. Journal of Hydraulic Research, 49, 424-436.
[50] Fredsøe, J. 1984. Turbulent boundary layer in wave-current motion. Journal of Hydraulic Engineering, 110, 1103-1120.
[51] Fredsøe, J., Andersen, K.H., Sumer, B.M., 1999. Wave plus current over a ripple-covered bed. Coastal Eng., 177–221.
[52] Fredsøe, J. and Deigaard, R., 1992. Mechanics of coastal sediment transport, 3. World scientific publishing company.
[53] Fuhrman, D.R., Fredsøe, J. and Sumer, B.M., 2009. Bed slope effects on turbulent wave boundary layers: 2. Comparison with skewness, asymmetry, and other effects. Journal of Geophysical Research: Oceans, vol. 114, no. C3, pp. C03025.
[54] Fuhrman, D.R., Schløer, S. and Sterner, J. 2013. RANS-based simulation of turbulent wave boundary layer and sheet-flow sediment transport processes. Coastal engineering, vol. 73, pp. 151-166.

[55] Glenn, S.M., 1983. A continental shelf bottom boundary layer model: The effects of waves, currents, and a movable bed. Doctoral dissertation, Massachusetts Institute of Technology and Woods Hole Oceanographic Institution.
[56] Gonzalez, F. I., and Rosenfeld, C. L., 1984. Slar and in situ observations of ocean swell modification by currents and bathymetry and the Columbia River entrance. IEEE Trans. Geosci. Remote Sens., GE-22(6), 598–603.
[57] Grant, W. D. and Glenn, S. M., 1983. Continental shelf bottom boundary layer model, Vol. II: Model/data comparison. WHOI Technical Report, 62.
[58] Grant, W.D. and Madsen, O.S., 1979. Combined Wave and Current Interaction with a Rough Bottom. Journal of Geophysical Research, 84, 1797-1808.
[59] Grant, W.D. and Madsen, O.S., 1986. The continental-shelf bottom boundary layer. Annual Review of Fluid Mechanics, 18, 265-305.
[60] Grigoriadis, D.G.E., Dimas, A.A., Balaras, E., 2012. Large-eddy simulation of wave turbulent boundary layer over rippled bed. Coastal Engineering, 60, 174–189.
[61] Groeneweg, J., Klopman, G., 1998. Changes of the mean velocity profiles in the combined wave–current motion described in a GLM formulation. Journal of Fluid Mechanics, 370, 271–296.
[62] Groeneweg, J., and Battjes, J.A., 2003. Three-dimensional wave effects on a steady current. Journal of Fluid Mechanics, 478, 325-343.
[63] Guillou, N., Chapalain, G. and Neill, S.P., 2016. The influence of waves on the tidal kinetic energy resource at a tidal stream energy site. Applied Energy, 180, 402-415.
[64] Guo, X. and Shen, L. 2013. Numerical study of the effect of surface waves on turbulence underneath. Part 1. Mean flow and turbulence vorticity. Journal of Fluid Mechanics, 733, 558-587.
[65] Hashemi, M.R., Grilli, S.T. and Neill, S.P., 2016. A simplified method to estimate tidal current effects on the ocean wave power resource. Renewable Energy, 96, 257-269.
[66] Hassan, W.N., Ribberink, J.S., 2005. Transport processes of uniform and mixed sands in oscillatory sheet flow. Coastal Engineering, 52, 745–770.
[67] Hedges, T.S. and Lee, B.W., 1992. The equivalent uniform current in wave-current computations. Coastal engineering, 16(3), 301-311.
[68] Henn, D.S., Sykes, R.I., 1999. Large-eddy simulation of flow over wavy surfaces. J. Fluid Mech., 75–112.
[69] Holmedal, L.E., Myrhaug, D., Rue, H., 2000. Seabed shear stresses under irregular waves plus current from Monte Carlo simulations of parameterized models, Coastal Engineering, 39, 123-147.
[70] Holmedal, L.E., Myrhaug, D., Rue, H., 2003. The sea bed boundary layer under random waves plus current. Continental Shelf Research, 23, 717–750.
[71] Holmedal, L.E. and Myrhaug, D. 2009. Wave-induced steady streaming, mass transport and net sediment transport in rough turbulent ocean bottom boundary layers. Continental shelf research, vol. 29, no. 7, pp. 911-926.
[72] Holmedal, L.E., Johari, J. and Myrhaug, D. 2013. The seabed boundary layer beneath waves opposing and following a current. Continental shelf research, vol. 65, pp. 27-44.
[73] Hsu, T.-J., Jenkins, J. T., and Philip, L.-F., 2004. On two-phase sediment transport: Sheet flow of massive particles, Proc. R. Soc. London A, 460, 2223–2250.
[74] Humbyrd, C.J., 2012. Turbulent combined wave-current boundary layer model for application in coastal waters. Ph.D. Thesis, Massachusetts Institute of Technology.
[75] Huntley, D.A., and Hazen, D.G., 1988. Seabed Stresses in Combined Wave and Steady Flow Conditions on the Nova Scotia Continental Shelf: Field measurements and Predictions. Journal of Physical Oceanography, 18, 347-362.

[76] Huynh-Thanh, S., and Temperville, A., 1991. A numerical model of the rough turbulent boundary layer in combined wave and current interaction. Coastal Engineering Proceedings, 1, 853-866.
[77] Jensen, B.L., 1989. Experimental and theoretical investigations in an oscillatory rough turbulent boundary layer. Series Pap. No. 44, Institute of Hydrodynamics and Hydraulic Eng., Technical University of Denmark, Lyngby, Denmark.
[78] Jepsen, R., Roberts, J., Kearney, S., Dimiduk, T., O'Hern, T., and Gailani, J., 2012. Shear Stress Measurements and Erosion Implications for Wave and Combined Wave-Current Generated Flows. Journal of Waterway, Port, Coastal, and Ocean Engineering, 138, 323–329.
[79] Jing, L. and Ridd, P.V., 1996. Wave-current bottom shear stresses and sediment resuspension in Cleveland Bay, Australia. Coastal Engineering, 29(1-2), pp.169-186.
[80] Jonsson, I.G and Carlsen, N.A., 1976. Experimental and theoretical investigations in an oscillatory rough turbulent boundary layer. J. Hydraul. Res., 14 (1): 45-60.
[81] Jonsson, I.G., Skougaard, C. and Wang, J.D., 1970. Interaction between waves and currents. Coastal Engineering Proceedings, 1(12).
[82] Jonsson, I. G., 1963. Measurements in the turbulent wave boundary layer. Int. Ass. Hydr. Res., 10th Congr., London 1963, vol. 1, 85-92.
[83] Jonsson, I.G., 1980. A new approach to oscillatory rough turbulent boundary layers. Ocean Engng., 7. 109-152.
[84] Jonsson, I.G., 1990. Wave current interactions. In: B. Le Mehaute and D.M. Hanes (Editors), The Sea, 9A. Wiley-Interscience, New York, pp. 65-120.
[85] Justesen, P., 1991. A note on turbulence calculations in the wave boundary layer. Journal of Hydraulic Research, 29, 699–711.
[86] Kajuira, K., 1968. A model for the bottom boundary layer in water waves. Bull. Earthquake Res. Inst., 45: 75-123.
[87] Kassem, S., and Ozkan-Haller, H. T., 2012. Forecasting the wave-current interactions at the Mouth of the Columbia River, or, USA, in 33rd International Conference on Coastal Engineering, Santander, Spain.
[88] Kemp, P. H. and Simons, R. R. 1982. The interaction between waves and a turbulent current: waves propagating with the current. Journal of Fluid Mechanics, 116, 227-250.
[89] Kemp, P. H. and Simons, R. R. 1983. The interaction of waves and a turbulent current: waves propagating against the current. Journal of Fluid Mechanics, 130, 73-89.
[90] Kirby, J.T., Chen, T., 1989. Surface waves on vertically sheared flows: approximate dispersion relations. J. Geophys. Res. 94, 1013–1027.
[91] Klopman, G., 1994. Vertical structure of the flow due to waves and currents: laser-Doppler flow measurements for waves following or opposing a current. Tech. Rep. Delft Hydraulics H840.32.
[92] Klopman, G., 1997. Secondary circulation of the flow due to waves and current: laser-Doppler flow measurements for waves following or opposing a current. Tech. Rep. Delft Hydraulics Z2249.
[93] Kukulka, T., Jenkins, R. L., Kirby, J. T., Shi, F., and Scarborough, R. W., 2017. Surface wave dynamics in Delaware Bay and its adjacent coastal shelf. Journal of Geophysical Research: Oceans, 122, 8683–8706.
[94] Kumar, N., Voulgaris, G. and Warner, J. C., 2011. Implementation and modification of a three-dimensional radiation stress formulation for surf zone and rip-current applications. Coastal Engineering, 58 (12), 1097-1117.
[95] Kumar, N., Voulgaris, G., Warner, J. C. & Olabarrieta, M., 2012. Implementation of the vortex force formalism in the coupled ocean-atmosphere-wave-sediment transport

(COAWST) modeling system for inner shelf and surf zone applications. Ocean Modelling, 47, 65-95.
[96] Lambrakos, K.F., Myrhaug, D. and Siaattelid, O.H., 1988. Seabed current boundary layers in wave-plus-current flow conditions. Journal of Waterway, Port, Coastal, and Ocean Engineering, 114(2), 161-174.
[97] Lewis, M., Neill, S.P., Robins, P., Hashemi, M.R. and Ward, S., 2017. Characteristics of the velocity profile at tidal-stream energy sites. Renewable Energy, 114, 258-272.
[98] Lim, K.Y. and Madsen, O.S., 2016. An experimental study on near-orthogonal wave–current interaction over smooth and uniform fixed roughness beds. Coastal Engineering, 116, 258-274.
[99] Lodahl, C.R., Sumer, B.M. and Fredsøe, J., 1998. Turbulent combined oscillatory flow and current in a pipe. Journal of Fluid Mechanics, 373, 313-348.
[100] Longuet-Higgins, M.S., 1953. Mass transport in water waves. Philosophical Transactions of the Royal Society of London Series, 245, 535–581.
[101] Longuet-Higgins, M.S. and Stewart, R.W., 1962. Radiation stress and mass transport in gravity waves, with application to 'surf beats'. Journal of Fluid Mechanics, 13(4), pp.481-504.
[102] Longuet-Higgins, M.S. and Stewart, R.W., 1964, August. Radiation stresses in water waves; a physical discussion, with applications. In Deep Sea Research and Oceanographic Abstracts (Vol. 11, No. 4, pp. 529-562). Elsevier.
[103] Lundgren, H., 1972. Turbulent currents in the presence of waves. Proc. 13th Coastal Engng. Conf., Vancouver, ASCE, chapter 33, 623-634.
[104] Lyne, V.D., Butman, B., Grant, W.D., 1990a. Sediment movement along the U.S. east coast continental shelf — I. Estimates of bottom stress using the Grant-Madsen model and near-bottom wave and current measurements. Continental Shelf Research, 10, 397–428.
[105] Lyne, V.D., Butman, B., Grant,W.D., 1990b. Sediment movement along the U.S. east coast continental shelf — II. Modelling suspended sediment concentration and transport rate during storms. Continental Shelf Research, 10, 429–460.
[106] MacIver, R.D., and Simons, R.R., 1997. Wave refraction on a horizontally sheared current in the UKCRF. In Coastal Dynamics, 425-435.
[107] Malarkey, J., Davies, A.G., 1998. Modelling wave–current interactions in rough turbulent bottom boundary layers. Ocean Engineering, 25, 119–141.
[108] Markus, D., Hojjat, M., Wuchner, R., and Bletzinger, K. U., 2013. A CFD Approach to Modelling Wave-Current Interaction. International Journal of Offshore and Polar Engineering, 23(1), 29-32.
[109] Mazzuoli, M., Vittori, G. and Blondeaux, P., 2011. Turbulent spots in oscillatory boundary layers. J. Fluid Mech., 685, 365–376.
[110] McWilliams, J. C., Restrepo, J. M. and Lane, E. M., 2004. An asymptotic theory for the interaction of waves and currents in coastal waters. Journal of fluid mechanics, 511, 135–178.
[111] Mellor, G., 2003. The three-dimensional current and surface wave equations. Journal of Physical Oceanography, 33(9), pp.1978-1989.
[112] Mellor, G.L., 2008. The depth-dependent current and wave interaction equations: a revision. Journal of Physical Oceanography, 38(11), pp.2587-2596.
[113] Mellor, G., 2011. Wave radiation stress. Ocean Dynamics, 61(5), pp.563-568.
[114] Mellor, G., 2015. A combined derivation of the integrated and vertically resolved, coupled wave–current equations. Journal of Physical Oceanography, 45(6), pp.1453-1463.

[115] Musumeci, R. E., Cavallaro, L., Foti, E., Scandura, P., & Blondeaux, P. (2006). Waves plus currents crossing at a right angle: Experimental investigation. Journal of Geophysical Research: Oceans, 111(C7).
[116] Myrhaug, D., 1982. On a theoretical model of rough turbulent wave boundary layers. Ocean Engineering, 9(6), 547-565.
[117] Myrhaug, D., 1984. A theoretical model of combined wave and current boundary layers near a rough sea bottom. Proc. 3rd, Offshore Mechanics and Arctic Engineering, OMAE Symp., New Orleans, LA., 1:559-568.
[118] Myrhaug, D., Reed, K. and Fyfe, A.J., 1987. Seabed boundary layer studies for pipelines: large scale laboratory experiments. Proc. 6th Int. Symp. Offshore Engineering, Rio de Janeiro, Brasil, pp. 345-359.
[119] Myrhaug, D. and Slaattelid, O.H., 1989. Combined wave and current boundary layer model for fixed rough seabeds. Ocean engineering, 16(2), 119-142.
[120] Myrhaug, D. and Slaattelid, O.H. 1990. A rational approach to wave-current friction coefficients for rough, smooth and transitional turbulent flow. Coastal Engineering, 14, 265-293.
[121] Myrhaug, D., Holmedal, L.E., Simons, R.R. and MacIver, R.D., 2001. Bottom friction in random waves plus current flow. Coastal Engineering, 43(2), 75-92.
[122] Nayak, A.R., Li, C., Kiani, B.T. and Katz, J., 2015. On the wave and current interaction with a rippled seabed in the coastal ocean bottom boundary layer. Journal of Geophysical Research: Oceans, 120(7), 4595-4624.
[123] Nepf, H.M. and Monismith, S.G., 1991. Experimental study of wave-induced longitudinal vortices. Journal of Hydraulic Engineering, ASCE, 117, 1639–1649.
[124] Nielsen, P., 1992. Coastal bottom boundary layers and sediment transport, 4, World Scientific Publishing Co. Pte. Ltd., Singapore.
[125] Nielsen, P., You, Z.J., 1996. Eulerian mean velocities under non-breaking waves on horizontal bottoms. In: Proc. 25th International Conference on Coastal Engineering (ICCE 1996), Orlando, FL, U.S.A, chapter 314, 4066–4078.
[126] O'Donoghue, T., Wright, S., 2004b. Flow tunnel measurements of velocities and sand flux in oscillatory sheet flow for well-sorted and graded sands. Coastal Engineering, 51, 1163–1184.
[127] Olabarrieta, M., Medina, R., Castanedo, S., 2010. Effects of wave–current interaction on the current profile, Coastal Engineering, 57, 643-655.
[128] Peregrine, D.H., 1967. Long waves on a beach, J. Fluid Mech., 27, 815–827.
[129] Peregrine, D.H., 1976. Interaction of water waves and currents. Advances in Applied Mechanics, 16, 9-117.
[130] Phillips, 1977. The Dynamics of the Upper Ocean. Cambridge University Press, 336 pp.
[131] Prandtl, L. 1925. Bericht über Untersuchungen zur ausgebildeten Turbulenz, Z. Angew. Math, Meth., 5, 136-139.
[132] Quinn, B.E., Toledo, Y., Shrira, V.I., 2017. Explicit wave action conservation for water waves on vertically sheared flows. Ocean Model., 112, 33–47.
[133] Ranasoma, K.M. and Sleath, J.F., 1994. Combined oscillatory and steady flow over ripples. Journal of waterway, port, coastal, and ocean engineering, 120(4), 331-346.
[134] Rapizo, H., Babanin, A.V., Provis, D. and Rogers, W.E., 2017. Current‐induced dissipation in spectral wave models. Journal of Geophysical Research: Oceans, 122(3), pp.2205-2225.
[135] Raushan, P.K., Singh, S.K., Debnath, K., Mukherjee, M. and Mazumder, B.S., 2018. Distribution of turbulent energy in combined wave current flow. Ocean Engineering, 167, 310-316.

[136] Roland, A and Ardhuin, F., 2014. On the developments of spectral wave models: numerics and parameterizations for the coastal ocean. Ocean Dynamics. 2014 Jun; 64(6):833-46.
[137] Ruessink, B.G., Michallet, H., Abreu, T., Sancho, F., Vander A., Werf, J.J., Silva, P.A., 2011. Observations of velocities, sand concentrations, and fluxes under velocity-asymmetric oscillatory flows. Journal of Geophysical Research 116, C03004.
[138] Rusu, L., Soares, C.G., 2011. Modelling the wave–current interactions in an offshore basin using the SWAN model. Ocean Engineering, 38, 63–76.
[139] Scandura, P., 2007. Steady streaming in a turbulent oscillating boundary layer. Journal of fluid mechanics, vol. 571, pp. 265-280.
[140] Simons, R.R., Grass, T.J., Tehrani, M.M., 1992. Bottom shear stresses in the boundary layers under waves and currents crossing at right angles. Coastal Engineering, chapter 45, 604-617.
[141] Simons, R.R., Grass, T.J., Saleh, W.M., Tehrani, M.M., 1994. Bottom shear stresses under random waves with a current superimposed. Coastal Engineering, chapter 42, 565-578.
[142] Simons, R.R., MacIver, R.D. and Saleh, W.M., 1997. Kinematics and shear stresses from combined waves and longshore currents in the UK coastal research facility. In Coastal Engineering 1996, 3481-3494.
[143] Simons, R.R. and MacIver, R.D., 2001. Regular, bichromatic and random waves on co-linear currents. In Coastal Dynamics' 01, 132-141.
[144] Simons, R.R., Myrhaug, D., Thais, L., Chapalain,G., Holmedal, L.E., and Maclver, R., 2000. Bed friction in combined wave-current flows. Coastal Engineering, 216-226.
[145] Singh, S.K. and Debnath, K., 2016. Combined effects of wave and current in free surface turbulent flow. Ocean Engineering, 127, 170-189.
[146] Singh, S.K., Debnath, K. and Mazumder, B.S., 2016. Spatially-averaged turbulent flow over cubical roughness in wave-current co-existing environment. Coastal Engineering, 114, 77-85.
[147] Singh, S.K., Raushan, P.K. and Debnath, K., 2018a. Turbulent characteristics of pulsating flow over hydraulically smooth surface. European Journal of Mechanics-B/Fluids, 68, 10-19.
[148] Singh, S.K., Raushan, P.K. and Debnath, K., 2018b. Combined effect of wave and current in rough bed free surface flow. Ocean Engineering, 160, 20-32.
[149] Singh, S.K., Raushan, P.K., Debnath, K. and Mazumder, B.S., 2018c. Higher order turbulent flow characteristics of oscillatory flow over a wall-mounted obstacle, ISH Journal of Hydraulic Engineering, 1-12.
[150] Skop, R. A., 1987. Approximate dispersion relation for wave-current interactions. J. Waterway, Port, Coastal, and Ocean Eng., 113, 187-195.
[151] Sleath, J.F.A., 1990a. Velocities and bed friction in combined flows. In Coastal Engineering 1990, 450-463.
[152] Sleath, J.F.A., 1990b. Seabed boundary layers. In: B. LeMehaute and D.M. Hanes (Editors), The Sea, 9. Wiley-Interscience, New York, pp. 693-727.
[153] Smagorinsky, J., 1963. General circulation experiments with the primitive equations. I: The basic experiments. Monthly Weather Review, 91, 99-164.
[154] Smith, J.D., 1977. Modelling of sediment transport on continental shelves. In: The Sea, vol. 6, Ed. By E.D. Goldberg et al. Wiley – Interscience, New York, pp. 539-577.
[155] Smith, J.A., 2006. Wave–current interactions in finite depth. Journal of Physical Oceanography, 36(7), 1403-1419.
[156] Soloviev, A.V., Hirons, A., Maingot, C., Dean, C.W., Dodge, R.E., Yankovsky, A.E., Wood, J., Weisberg, R.H., Luther, M.E. and McCreary, J.P., 2017. Southward flow on

the western flank of the Florida Current. Deep Sea Research Part I: Oceanographic Research Papers, 125, 94-105.
[157] Son, S. and Lynett, P.J., 2014. Interaction of dispersive water waves with weakly sheared currents of arbitrary profile. Coastal Engineering, 90, 64-84.
[158] Soulsby, R.L., Hamm, L., Klopman, G., Myrhaug, D., Simons, R.R., and Thomas, G.P. 1993. Wave-current interaction within and outside the bottom boundary layer. Coastal Engineering, 21, 41–69.
[159] Soulsby, R. L. and Humphrey, J. D., 1990. Field observations of wave–current interaction at the sea bed. In Proceedings of the NATO Advanced Research Workshop on Water Wave Kinematics, ed. A. Tørum and O. T. Grudmestad, 413-428. Kluwer, Dordrecht.
[160] Sumer, B.M., Jensen, B.L. and Fredsoe, J., 1986. In Advances in Turbulences, pp. 556-567.
[161] Sumer, B.M., Laursen, T.S., Fredsøe, J., 1993. Wave boundary layer in a convergent tunnel. Coastal Engineering, 20, 317–342.
[162] Swan, C., 1990. An experimental study of waves on a strongly sheared current profile. In Proceedings of 22nd International Conference on Coastal Engineering, Delft, The Netherlands, 489-502.
[163] Tambroni, N., Blondeaux, P. and Vittori, G., 2015. A simple model of wave–current interaction. Journal of Fluid Mechanics, 775, 328-348.
[164] Teles, M. J., Pires-Silva, A., and Benoit, M., 2012. The influence of the turbulence closure model on wave-current interaction modelling at a local scale. Proceedings of 33rd Conference on Coastal Engineering, Santander, Spain, 1-12.
[165] Teles, M.J., Pires-Silva, A.A., Benoit, M., 2013. Numerical modelling of wave current interactions at a local scale. Ocean Modelling, 68, 72–87.
[166] Thomas, G.P., 1981. Wave-current interactions: an experimental and numerical study. Part 1. Linear waves. Journal of Fluid Mechanics, 110, 457-474.
[167] Thomas, G.P., 1990. Wave–current interactions: an experimental and numerical study. Part 2. Nonlinear waves. Journal of Fluid Mechanics, 216, 505-536.
[168] Thomson, J., Horner-Devine, A. R., Zippel, S., Rusch, C. and Geyer, W., 2014. Wave breaking turbulence at the offshore front of the Columbia River Plume. Geophys. Res. Lett., 41, 8987–8993.
[169] Tolman, H.L., 1990. The influence of unsteady depths and currents of tides on wind-wave propagation in shelf seas. Journal of Physical Oceanography, 20(8), 1166-1174.
[170] Trowbridge, J.H. and Agrawal, Y.C., 1995. Glimpses of a wave boundary layer. Journal of Geophysical Research: Oceans, 100(C10), 20729-20743.
[171] Trowbridge, J.H., Madsen, O.S., 1984. Turbulent wave boundary layers: 2. Second-order theory and mass transport. J. Geophys. Res. 89 (C5), 7999–8007.
[172] Umeyama, M., 2005. Reynolds Stresses and Velocity Distributions in a Wave-Current Coexisting Environment. Journal of Waterway, Port, Coastal, and Ocean engineering, 131, 203-212.
[173] Umeyama, M., 2009. Changes in Turbulent Flow Structure under Combined Wave-Current Motions. Journal of Waterway, Port, Coastal, and Ocean Engineering, 135, 213–227.
[174] Umeyama, M., 2011. Coupled PIV and PTV Measurements of Particle Velocities and Trajectories for Surface Waves Following a Steady Current. Journal of Waterway, Port, Coastal, and Ocean Engineering, 137, 85–94.
[175] Umeyama, M. and Gerritsen, F., 1992. Velocity distribution in uniform sediment-laden flow. Journal of Hydraulic Engineering, 118(2), 229-245.

[176] van der Westhuysen, A., Lesser, G., 2007. Evaluation and Development of Wave-Current Interaction in SWAN: activity 6.4 of SBW project Waddenzee Tech. Rep. Deltares (WL).
[177] Van Doom, Th., 1981. Experimental investigation of near bottom velocities in water waves with and without a current. Delft Hydraulics Laboratory, Tow-Report 1423.
[178] Van Doorn, Th., 1982. Experimenteel onderzoek naar het snelheidsveld in de turbulente bodemgrenslaag in een oscillerende stroming in een goletunnel. Delft Hydraulics Laboratory, Report No. M1562-1a.
[179] Visser, P.J., 1986. Wave basin experiments on bottom friction due to current and waves. In Coastal Engineering 1986, 807-821.
[180] Vittori, G. and Verzicco, R., 1998. Direct simulation of transition in an oscillatory boundary layer. J. Fluid Mech., 371, 207–232.
[181] Wiberg, P. and Smith, J.D., 1983. A comparison of field data and theoretical models for wave-current interactions at the bed on the continental shelf. Continental Shelf Research, 2(2-3), pp.147-162.
[182] Wolf, J. and Prandle, D., 1999. Some observations of wave–current interaction. Coastal Engineering, 37, 471–485.
[183] Yang, Z.T. and Liu, P.L.F., 2020. Depth-integrated wave-current models. Part 1. Two-dimensional formulation and applications, Journal of fluid mechanics, vol. 883, A4.
[184] Yang, D. and Shen, L., 2009. Characteristics of coherent vortical structures in turbulent flows over progressive surface waves. Physics of Fluids, 21, 125106 (1-23).
[185] Yang, S., Tan, S.K., Lim, S.Y., Zhang, S.F., 2006. Velocity distribution in combined wave–current flows. Advances in Water Resources, 29, 1196–1208.
[186] Yoon, S.B., Liu, P.L.F., 1989. Interaction of current and weakly nonlinear water waves in shallow water, J. Fluid Mech., 205, 71–92.
[187] You, Z.J., 1994a. Eddy viscosities and velocities in combined wave-current flows. Ocean engineering, 21(1), 81-97.
[188] You, Z.J., 1994b. A simple model for current velocity profiles in combined wave-current flows. Coastal Engineering, 23(3-4), 289-304.
[189] You, Z.J., 1996. The effect of wave-induced stress on current profiles. Ocean engineering, 23, 619-628.
[190] You, Z.J., Wilkinson, D.L. and Nielsen, P., 1991. Velocity distributions of waves and currents in the combined flow. Coastal Engineering, 15(5-6), 525-543.
[191] You, Z.J., Wilkinson, D.L., and Nielsen, P., 1992. Velocity distribution in turbulent oscillatory boundary layer. Coastal engineering, 18, 21-38.
[192] Yu, X., Hsu, T.-J., Hanes, D.M., 2010. Sediment transport under wave groups: relative importance between nonlinear wave shape and nonlinear boundary layer streaming. Journal of Geophysical Research 115, C02013.
[193] Yuan, J. and Madsen, O.S., 2015. Experimental and theoretical study of wave–current turbulent boundary layers. Journal of Fluid Mechanics, 765, 480-523.
[194] Zhang, J.S., Zhang, Y., Jeng, D.S., Liu, P.L.F., Zhang, C. 2014. Numerical simulation of wave–current interaction using a RANS solver. Ocean Engineering, 75, 157-164.
[195] Zhang, X., Simons, R. and Buldakov, E., 2017. A numerical study of wave-current interaction in the bottom boundary layer. In Proceedings of 35th International Conference on Coastal Engineering, 35.
[196] Zhu, Q., van Prooijen, B.C., Wang, Z.B., Ma, Y.X. and Yang, S.L., 2016. Bed shear stress estimation on an open intertidal flat using in situ measurements. Estuarine, Coastal and Shelf Science, 182, pp.190-201.

[197] Zippel, S., and Thomson, J., 2017. Surface wave breaking over sheared currents: Observations from the Mouth of the Columbia River, J. Geophys. Res. Oceans, 122, 3311–3328.
[198] Zou, Z.L., Hu, P.C., Fang, K.Z., and Liu, Z.B., 2013. Boussinesq-type equations for wave–current interaction. Wave Motion, 50, 655–675.
[199] Zheng, J., Yao, Y., Chen, S., Chen, S., Zhang, Q. Laboratory study on wave-induced setup and wave-driven current in a 2DH reef-lagoon-channel system. Coastal Engineering, 2020, 162, 103772.
[200] Zheng, J., Zhang, C., Demirbilek, Z., Lin, L. Numerical study of sandbar migration under wave-undertow interaction. Journal of Waterway, Port, Coastal and Ocean Engineering, 2014, 140(2): 146–159.
[201] Zhang, C., Zheng, J., Zhang, J. Predictability of wave-induced net sediment transport using the conventional 1DV RANS diffusion model. Geo-Marine Letters, 2014, 34(4):353-364.